# Feynman Diagrams

## Fully Relativistic

## Four Papers in Physical Review

**The theory of positrons (1949)**

**Space-Time Approach to Quantum Electrodynamics (1949)**

**Mathematical formulation of the quantum theory of electromagnetic interaction (1950)**

**An Operator Calculus Having Applications in Quantum Electrodynamics (1951)**

## Lecture Notes

**Quantum Electrodynamics**
**Benjamin Press (1961)**

# GENIUS

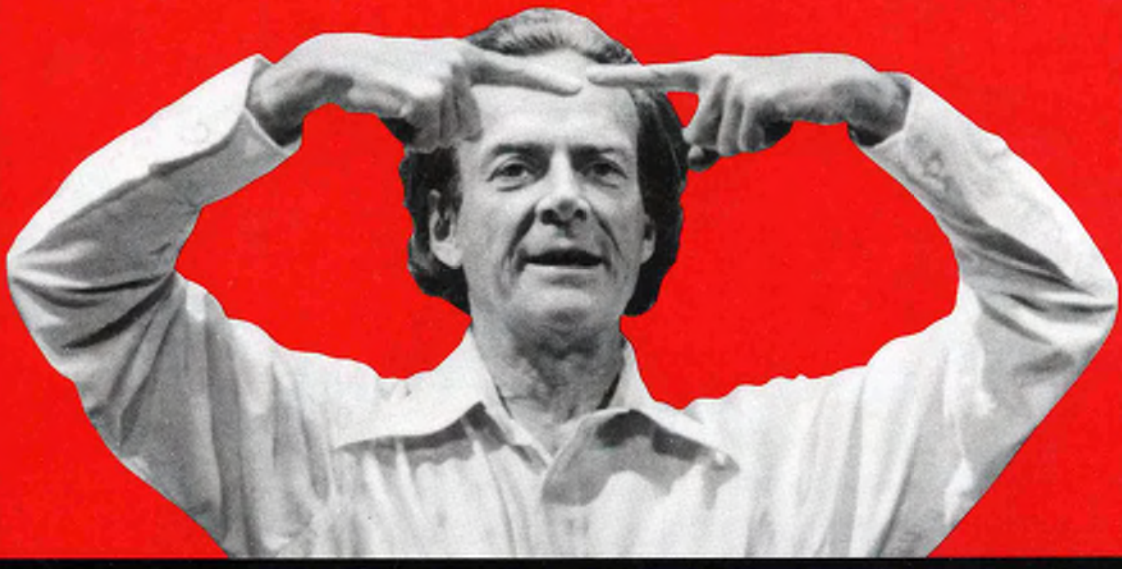

## THE LIFE AND SCIENCE OF RICHARD FEYNMAN

JAMES GLEICK

AUTHOR OF CHAOS

# THE BEAT OF A DIFFERENT DRUM

*The life and science of Richard Feynman*

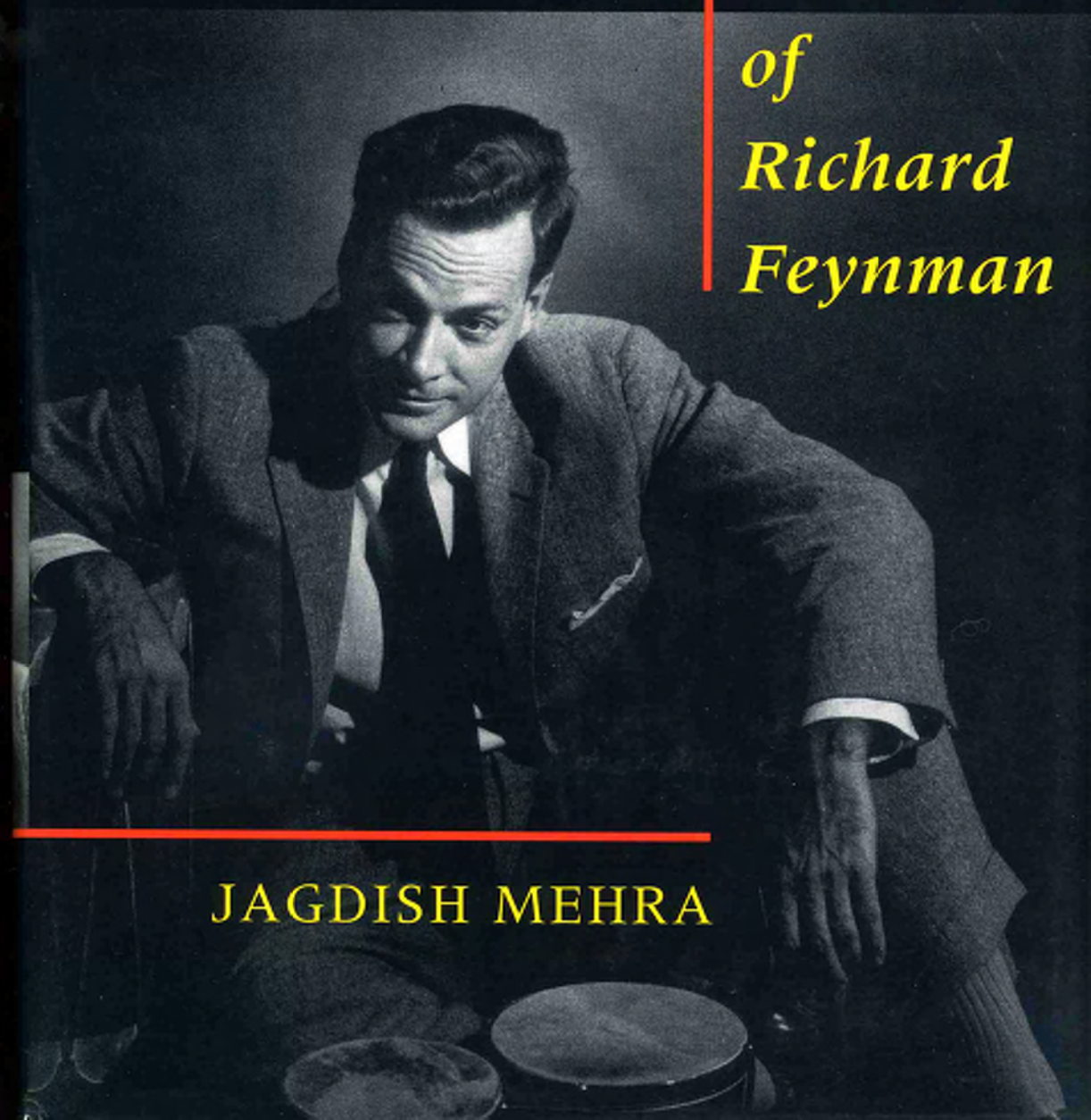

JAGDISH MEHRA

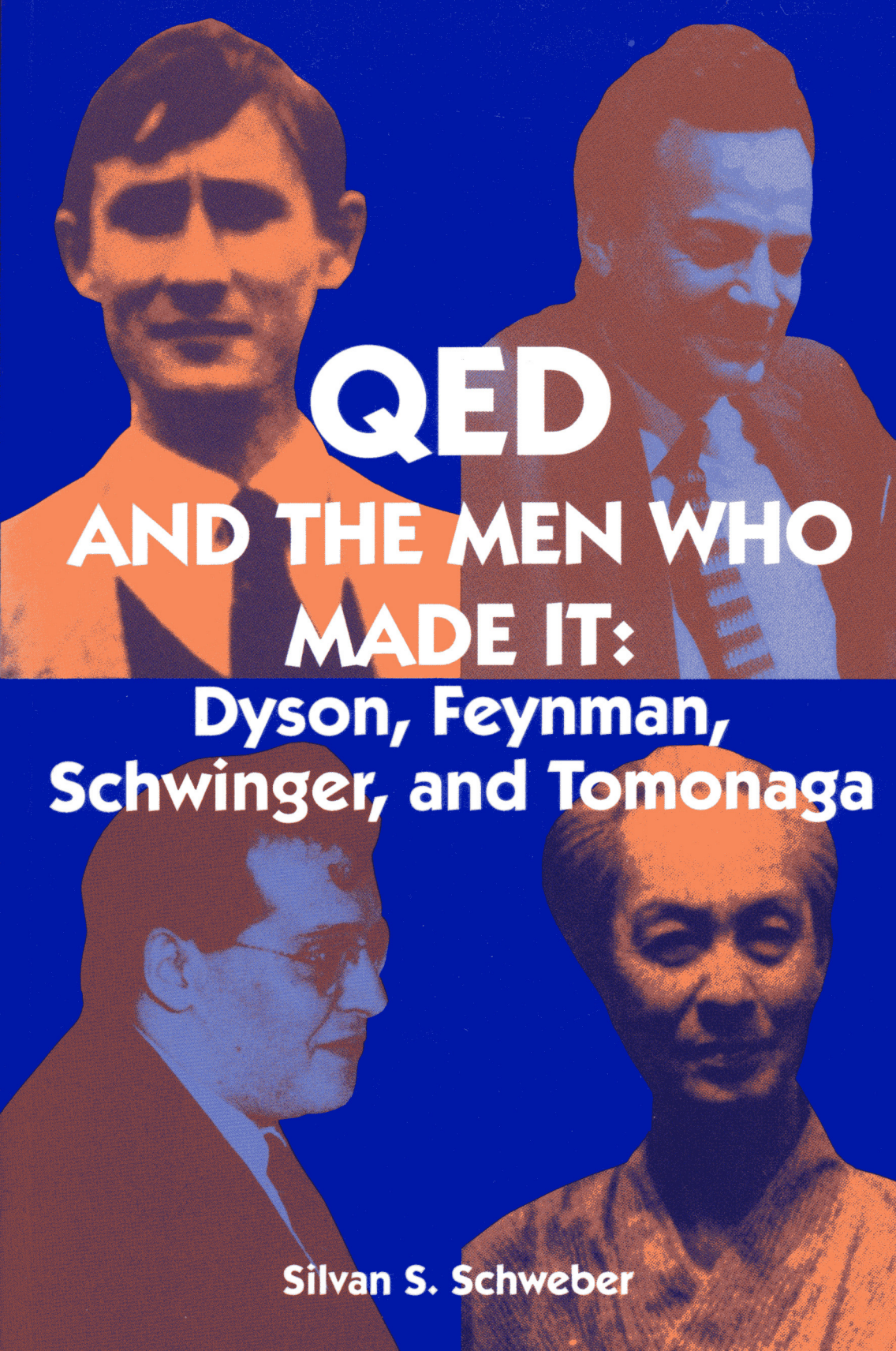

# QED

## AND THE MEN WHO MADE IT:

## Dyson, Feynman, Schwinger, and Tomonaga

Silvan S. Schweber

## *Around a Mental Block*

Princeton was celebrating the bicentennial of its founding with a grand explosion of pomp that fall: parties, processions, and a series of formal conferences that drew scholars and dignitaries from long distances. Dirac had agreed to speak on elementary particles as part of a three-day session on the future of nuclear science. Feynman was invited to introduce his one-time hero and lead a discussion afterward.

He disliked Dirac's paper, a restatement of the now-familiar difficulties with quantum electrodynamics. It struck him as backward-looking in its Hamiltonian energy-centered emphasis—a dead end. He made so many nervous jokes that Niels Bohr, who was due to speak later in the day, stood up and criticized him for his lack of seriousness. Feynman made a heartfelt remark about the unsettled state of the theory. "We need an intuitive leap at the mathematical formalism, such as we had in the Dirac electron theory," he said. "We need a stroke of genius."

As the day wore on—Robert Wilson speaking about the high-energy scattering of protons, E. O. Lawrence lecturing on his California accelerators—Feynman looked out the window and saw Dirac lolling on a patch of grass and gazing at the sky. He had a question that he had wanted to ask Dirac since before the war. He wandered out and sat down. A remark in a 1933 paper of Dirac's had given Feynman a crucial clue toward his discovery of a quantum-mechanical version of the *action* in classical mechanics. "It is now easy to see what the quantum analogue of all this must be," Dirac had written, but neither he nor anyone else had pursued this clue until Feynman discovered that the "analogue" was, in fact, exactly proportional. There was a rigorous and potentially useful mathematical bond. Now he asked Dirac whether the great man had known all along that the two quantities were proportional.

"Are they?" Dirac said. Feynman said yes, they were. After a silence he walked away.

Feynman's reputation was traveling around the university circuit. Job offers floated his way. They seemed perversely inappropriate and did nothing to help his mood of frustration. Oppenheimer had invited him to California for the spring semester; now he turned the invitation down. Cornell promoted him to associate professor and raised his salary again. The chairman of the University of Pennsylvania's physics department needed a new chief theorist. Here Bethe stepped in paternalistically: he had no intention of

**Many years later Feynman and Dirac met one more time. They exchanged a few awkward words---a conversation so remarkable that a physicist within earshot immediately jotted down the Pinteresque dialog he thought drifting his way:**

**I am Feynman.**

**I am Dirac.**

**(Silence)**

**It must be wonderful to be the discoverer of that equation.**

**That was a long time ago. (Pause) What are you working on?**

**Mesons.**

**Are you trying to discover an equation for them?**

**It is very hard.**

**One must try.**

and just calculated the integral by means of the Taylor series expansion, thus working out the Schrödinger equation

$$\left(-\frac{\hbar^2}{2m}\frac{\partial^2}{dx^2}+V(x)\right)\psi(x,t)=i\hbar\frac{\partial}{\partial t}\psi(x,t). \tag{6.12}$$

Feynman turned to Jehle, who did not quite follow, and told him that Dirac meant that they were proportional. Herbert Jehle had taken out a little notebook and was rapidly copying it down from the blackboard, and said, 'No, no, this is an important discovery. You Americans are always trying to find out how something can be used. That's a good way to discover things!'[22]

In the fall of 1946, Princeton University was celebrating its bicentennial, on the occasion of which numerous festivities, including various series of lectures were organized. In one of these sessions, devoted to science and organized by Eugene Wigner, Feynman was invited to introduce Dirac and, after his lecture, comment upon it. 'It was like the ward-heeler of the 54th district (in New York City) introducing the president of the United States. Dirac sent me his paper, in his own handwriting, to read and I had to comment on it. After Dirac's lecture, I made my comments; I tried to simplify Dirac's very technical talk for the benefit of high school teachers and others who were not familiar with the things that Dirac had talked about. But the other physicists, like Bohr and Weisskopf, who were there did not give a damn about these other people, and they criticized my attempt to 'explain Dirac' in my simplified way. After I had made my criticism, people were standing around and discussing Dirac's paper, and I looked through the window and saw that Dirac was lying on the lawn outside looking up in the sky. I had never really sat and talked to him before then. But there was this question which I very much wanted to ask him, so I walked up to him and said: 'Professor Dirac, you wrote in a paper[23] in which you talk about the analogy between exp $(i\varepsilon L)$ and the difference between two points. He said, "yes." I said, "Did you know that they are not just analogous, they are equal or rather proportional." He said, "Are they?" I said, "Yes." "Oh, that's interesting," was his comment. I wanted to know whether I had discovered something or not, but he had never sat down to find out whether they were equal or proportional. He just said, "No, I didn't know, are they? That's interesting!" That was the first time I talked to him personally.'[1]

In his paper Dirac was not able to complete this line of his investigations on quantum mechanics because his point of view was based on the opinion that the correspondence between the function $K$ and the exponent of the classical action function is only an approximate semiclassical relation. From the very beginning of relativistic quantum mechanics it had been recognized that the expression $\exp[(i/\hbar)S]$ gave the semiclassical approximation to the exact quantum wave function. Therefore Dirac was looking for a proper and exact quantum analog of Hamilton's principal function $S$, and he found relations between the corresponding exact quantum Hamiltonian wave function and

NO ELECTRIC FIELDS
NO MAGNETIC FIELDS

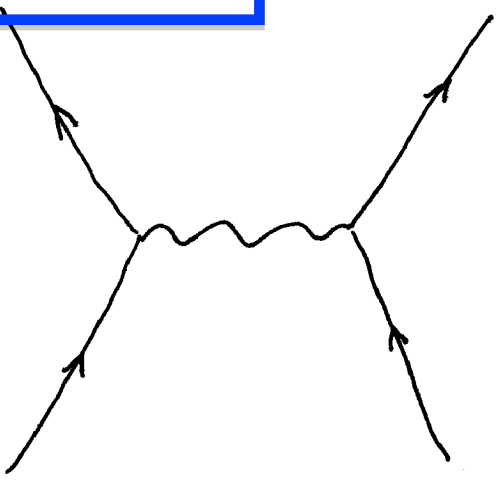

VIRTUAL PHOTON EXCHANGE

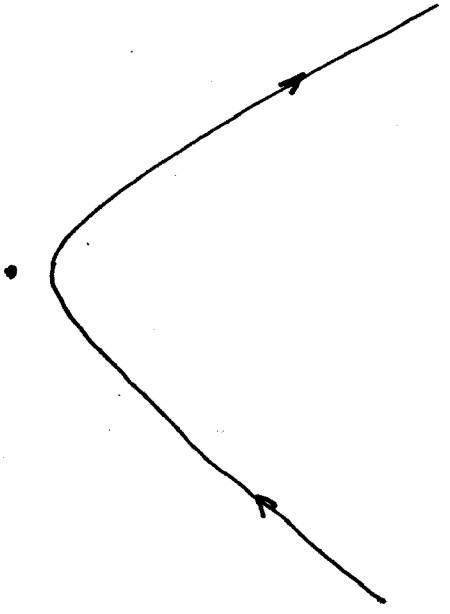

COULOMB

POTENTIAL

$\Delta E \, \Delta t \sim \hbar/2$

BREMSSTRALUNG

SYNCHROTRON RADIATION

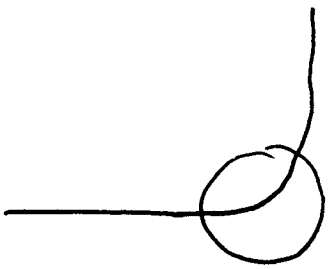

SHARP BEND

LARGE ACCELERATION

LOTS OF RADIATION

QED

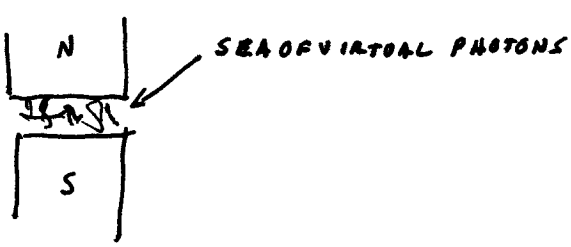


COLLISION WITH e MAKES ONE REAL

| | | | |
|---|---|---|---|
| PHOTON | $E = pc$ | $E^2 = p^2c^2$ | REAL |
| | $E \neq pc$ | | VIRTUAL |
| ELECTRONS | $E^2 = p^2c^2 + m_0^2c^4$ | | REAL |
| | $E^2 \neq$ | | VIRTUAL |
| | | | OFF MASS SHELL |

REAL PHOTONS LIVE FOREVER MACROSCOPIC DISTANCE

" ELECTRONS " "

VIRTUAL PARTICLES DO NOT

$$\Delta E \, \Delta t \geq \frac{\hbar}{2}$$

$$\Delta t \simeq \frac{\hbar}{2 \Delta E}$$

$$d = v\, t = c \frac{\hbar}{2E}$$

LARGE ENERGY => SHORT DISTANCE

SMALL ENERGY => LONG DISTANCE

COULOMB SCATTERING

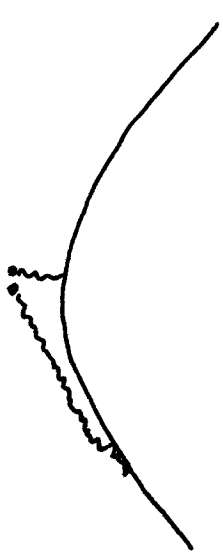

FORCE BETWEEN 2 ELECTRONS ...

# BREMSSTRAHLUNG

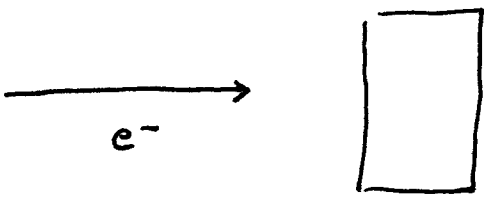


SUDDEN STOP

LARGE ACCELERATION

LOTS OF RADIATION

QED

SAME FINAL STATE

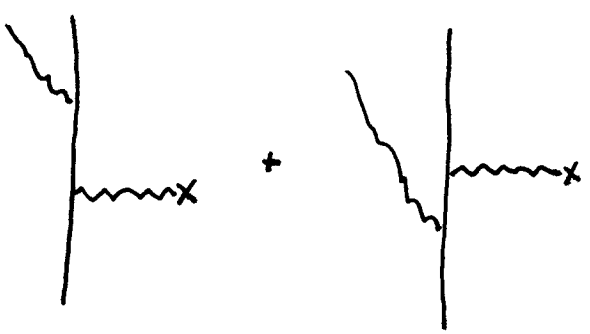

NUCLEUS SCATHING WITH VIRTUAL ~~ELECTRONS~~ PHOTONS

COLLISION WITH ELECTRON MAKES ONE REAL

ONLY REAL PHOTONS TRAVEL TO ∞

PAIR PRODUCTION NEAR NUCLEI

BREMSSTRAHLUNG HOLOGRAPHY


CRYSTAL

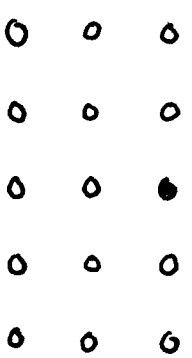

INTERFERENCE PATTERN

⇓

CRYSTAL STRUCTURE

## BREMSTRAHLUNG SOURCE

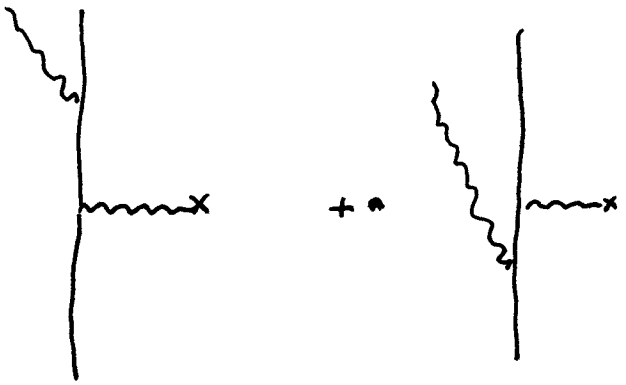

SAME FINAL STATE => INTERFERE

## COMPTON SCATTERING

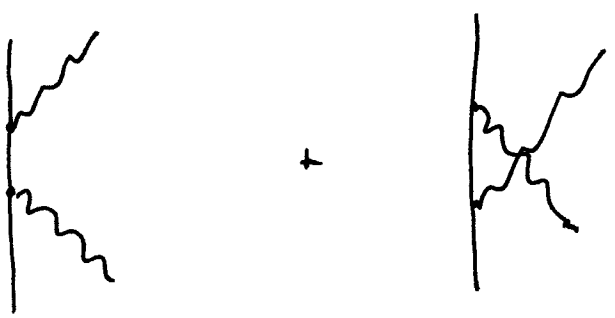

SAME FINAL STATE => INTERFERE

FOUR DIAGRAMS

# Four Diagrams

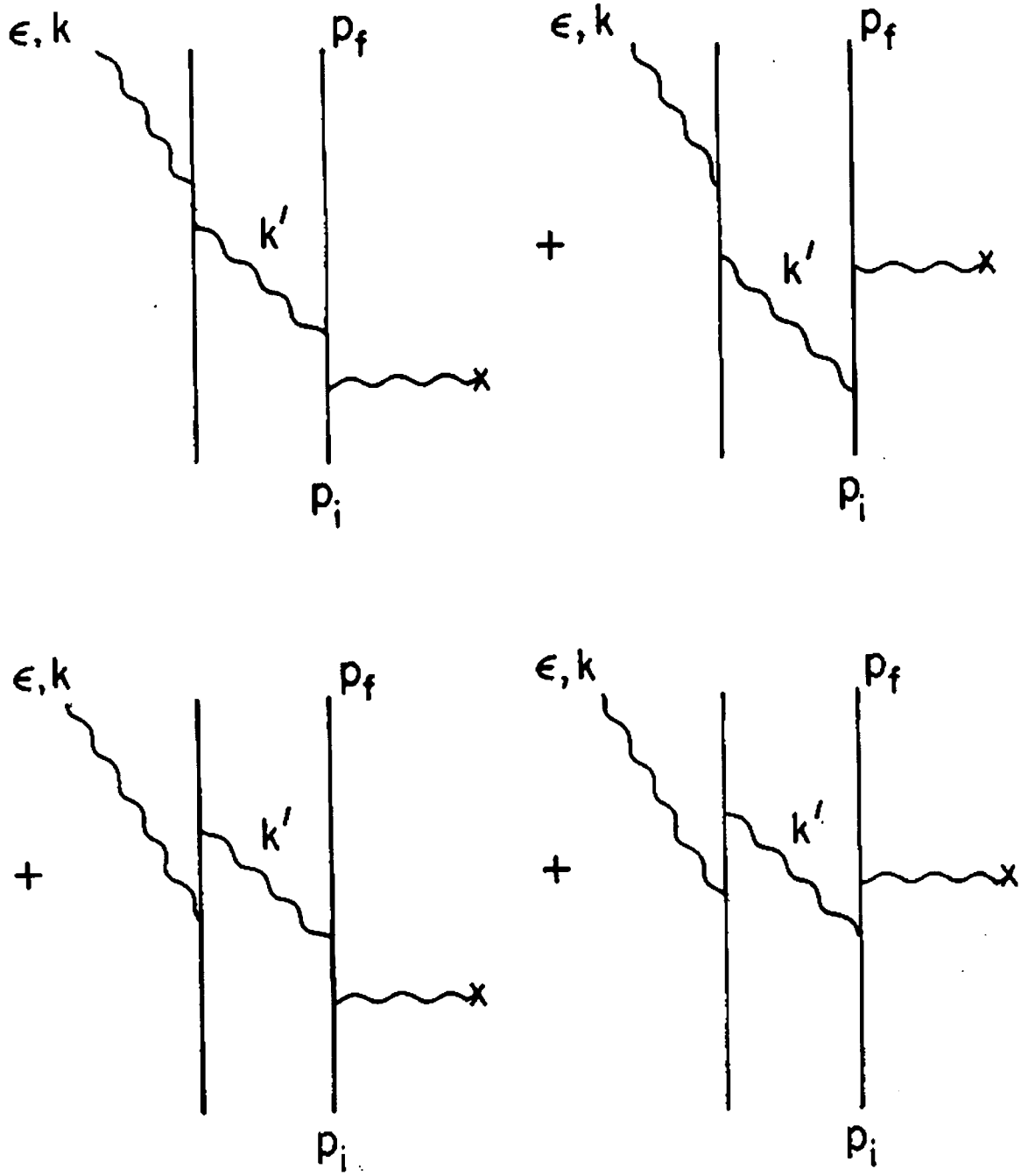

JUST LIKE DIRAC NOTATION, AT SOME POINT SOME ONE MUST DO THE INTEGRALS...

PROPAGATORS


$$\int d^4k \quad \frac{1}{k^2 + i\epsilon}$$

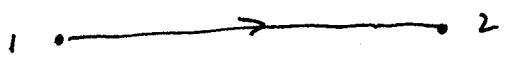


$$\int d^4p \quad \frac{m + p}{m^2 - p^2 - i\epsilon}$$

PRB 56, 2399 (1997).

# Quantum electrodynamics of the internal source x-ray holographies: Bremsstrahlung, fluorescence, and multiple-energy x-ray holography

Gerald A. Miller and Larry B. Sorensen
*Department of Physics, University of Washington, Seattle, Washington 98195*
(Received 19 November 1996)

Quantum electrodynamics (QED) is used to derive the differential cross sections measured in the three new experimental internal source ensemble x-ray holographies: bremsstrahlung (BXH), fluorescence (XFH), and multiple-energy (MEXH) x-ray holography. The polarization dependence of the BXH cross section is also obtained. For BXH, we study analytically and numerically the possible effects of the virtual photons and electrons which enter QED calculations in summing over the intermediate states. For the low photon and electron energies used in the current experiments, we show that the virtual intermediate states produce only very small effects. This is because the uncertainty principle limits the distance that the virtual particles can propagate to be much shorter than the separation between the regions of high electron density in the adjacent atoms. We also find that using the asymptotic form of the scattering wave function causes about a 5–10 % error for near forward scattering. [S0163-1829(97)01622-6]

## I. INTRODUCTION

Fifty years ago, Gabor proposed electron holography as a method to improve the resolution of electron microscopes so that atoms could be directly imaged.[1] Gabor's idea was to focus the electron beam to a very small region of space just outside the sample to produce a nearly point source of radiation, and to record the interference pattern between the spherical reference wave from this point source and the spherical object waves produced when the electrons scattered from the atoms in the sample. This photographically recorded interference pattern would then be used as the diffraction grating in an optical reconstruction system. Although Gabor's dream to directly image atoms using holographic electron microscopy has never been realized (because the quality of the best electron lenses is only about as good as that of a raindrop for visible light[2]), Gabor's suggestion produced the optical holography revolution with the advent of lasers to provide the necessary coherent monochromatic external reference waves.

Ten years ago, Szöke pointed out that the necessary coherent spherical reference wave could also be created by generating the electron reference wave inside the sample.[3] In this case, the spatial coherence comes from the small spatial extent of the internal electron source. Szöke's internal source electron holography suggestion generated a flurry of activity,[4] and, in the past five years, Gabor's dream of directly imaging atoms with electrons has been partially realized for atoms within the first few atomic layers of the surface of a crystal using photoelectrons,[5] Auger electrons,[6] diffusely scattered low energy electrons,[7] and diffusely scattered Kikuchi electrons.[8] However, because electrons interact very strongly with atoms, the scattered object waves are not very good spherical waves (there is a strong angular variation of the magnitude and the phase of the electron-atom scattering amplitude), and multiple scattering produces ''electron focusing'' effects along the lines of atoms in the sample which are important. Consequently, these new electron holographies produce pictures of where the atoms are, but they do not accurately reconstruct the atomic positions. Szöke also proposed internal source x-ray holography using fluorescence x rays. Because x rays interact weakly with atoms, internal source x-ray holograms should produce much more accurate atomic resolution images than the internal source electron holographies.[9,10] Unfortunately, the price for this is that the modulation of the intensity in x-ray holograms $(1-5\times10^{-3})$ is about 100 times weaker than the modulation in electron holograms $(1-5\times10^{-1})$.

Earlier this year, the first atomic resolution x-ray holograms were produced using x-ray fluorescence holography[11] (XFH) and multiple-energy x-ray holography (MEXH).[12] About three years ago, stimulated by the advantages of multiple-energy electron holography[13] and the promise of XFH,[9] we started developing a new kind of internal source x-ray holography which uses bremsstrahlung photons created inside the sample.[14] The primary motivation for this paper is to provide the theoretical foundation for experimental bremsstrahlung x-ray holography (BXH) starting from quantum electrodynamics. The bulk of this paper is devoted to BXH, but we also show how the same quantum electrodynamic foundation applies to XFH and MEXH.

Bremsstrahlung x-ray holography is very attractive for three reasons: (1) Bremsstrahlung allows hard x rays to be produced from low $Z$ atoms. High quality holograms require the wavelength to be much smaller than the spacing between the atoms. The characteristic fluorescence energies of many interesting and important low $Z$ elements are too low to provide good images using XFH. (2) Bremsstrahlung produces x rays with a wide spread in their energy and allows multiple energy holograms to be recorded simultaneously by energy analyzing the bremsstrahlung photons. To accurately reconstruct a three-dimensional object in real space, we need information over a three-dimensional volume in reciprocal space. To overcome the problems in the internal source single-energy electron holographies, several multiple-energy methods have been developed.[13] These multiple-energy elec-

 

# Holography 101

## Recording Step

$$\text{Intensity} = |R + O|^2 = R^*R + R^*O + RO^* + O^*O$$


## Playback Step

$$I = R\,|\,R + O\,|^2 = RR^*R + RR^*O + RRO^* + RO^*O$$

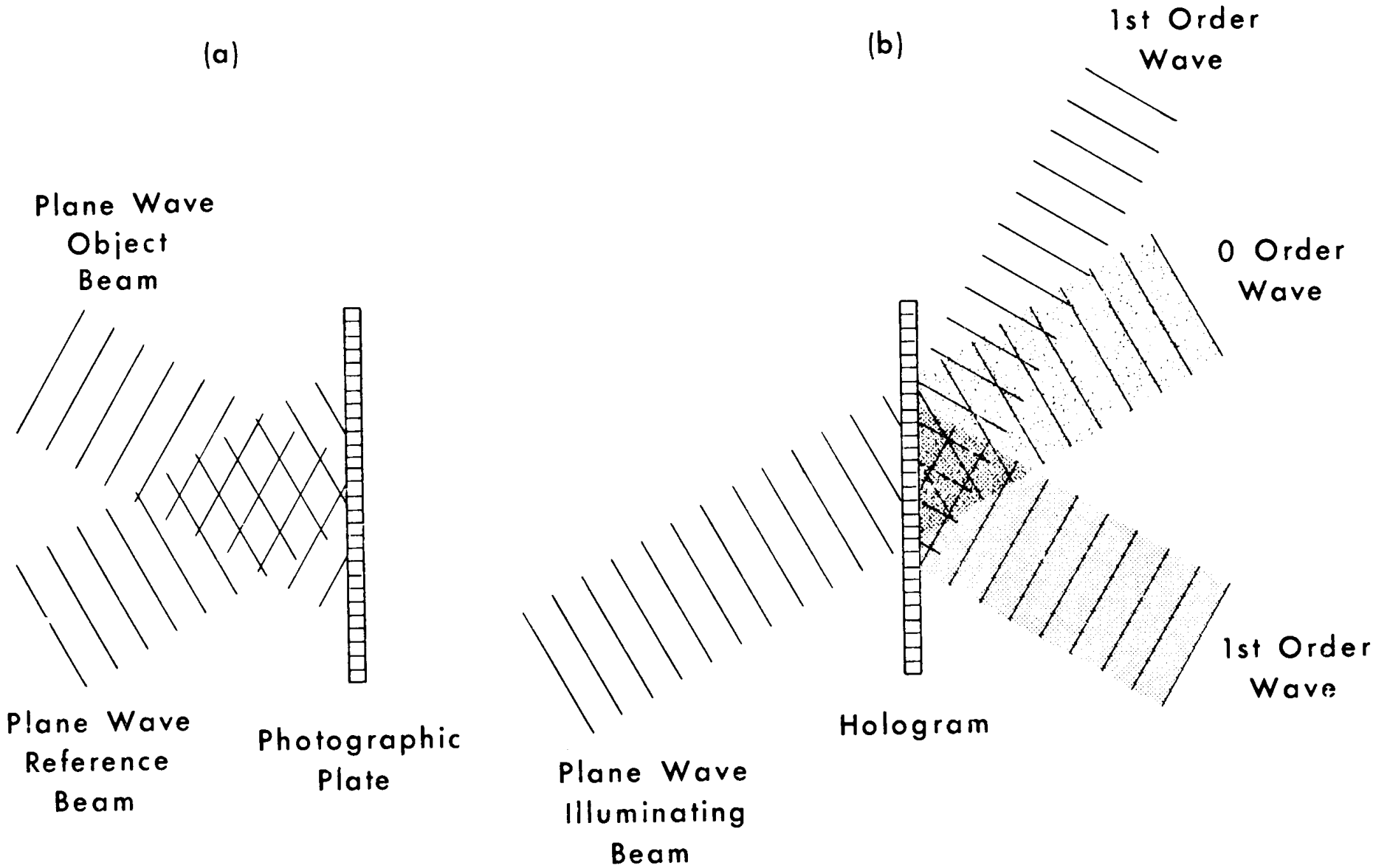


**Fig. 2.1** The basic plane wave hologram. (*a*) Recording the two-beam interference pattern. (*b*) The diffraction of a plane wave from the recorded interference pattern.

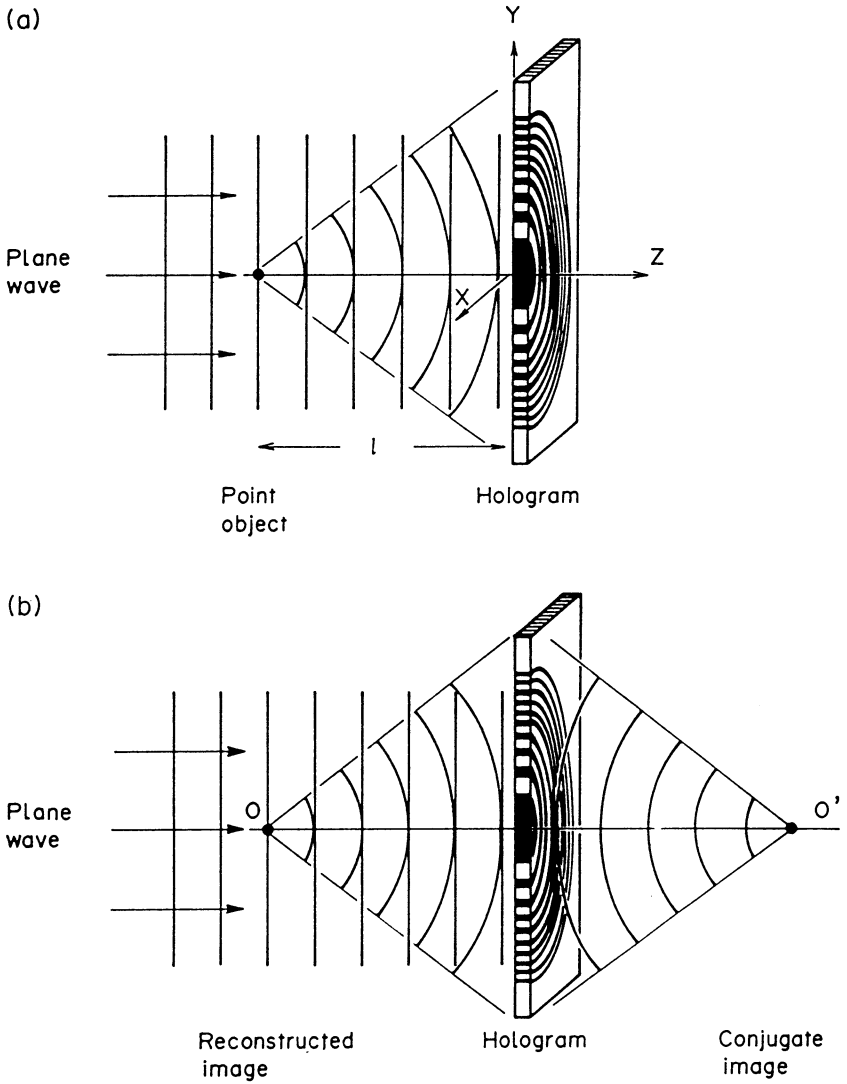


**Fig.2.1.** In-line holography of a point object: (**a**) Hologram formation, and (**b**) image reconstruction

The first and second terms here represent the transmitted plane waves. The third term gives the original wave scattered from the point object, that is, a spherical wave diverging from point O (Fig.2.1b). The fourth term represents a spherical wave converging to the point O′, located at the position mirror-symmetric to the point O with respect to the hologram plane. This fourth term describes the conjugate image.

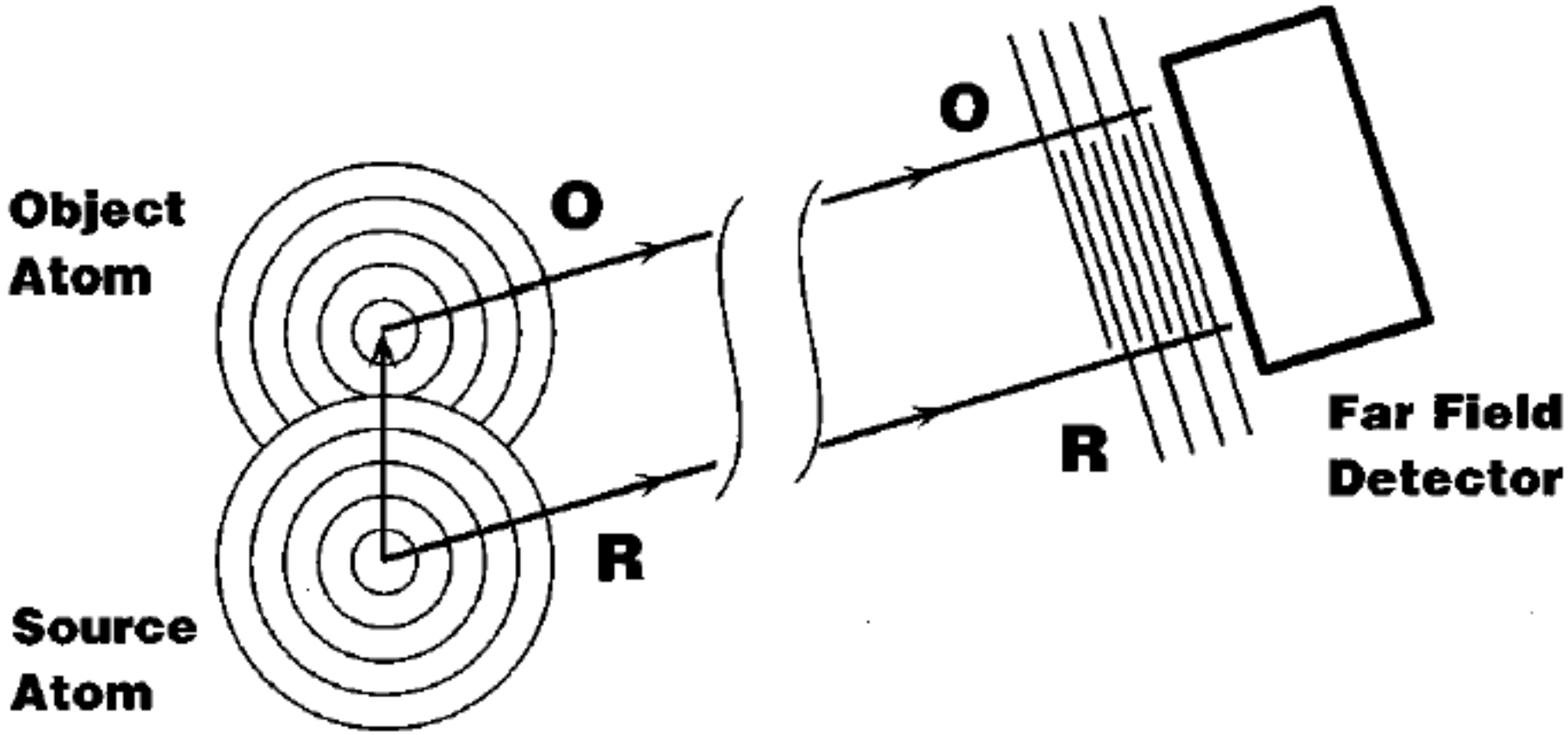
Object
Atom
O
R
Source
Atom
O
R
Far Field
Detector

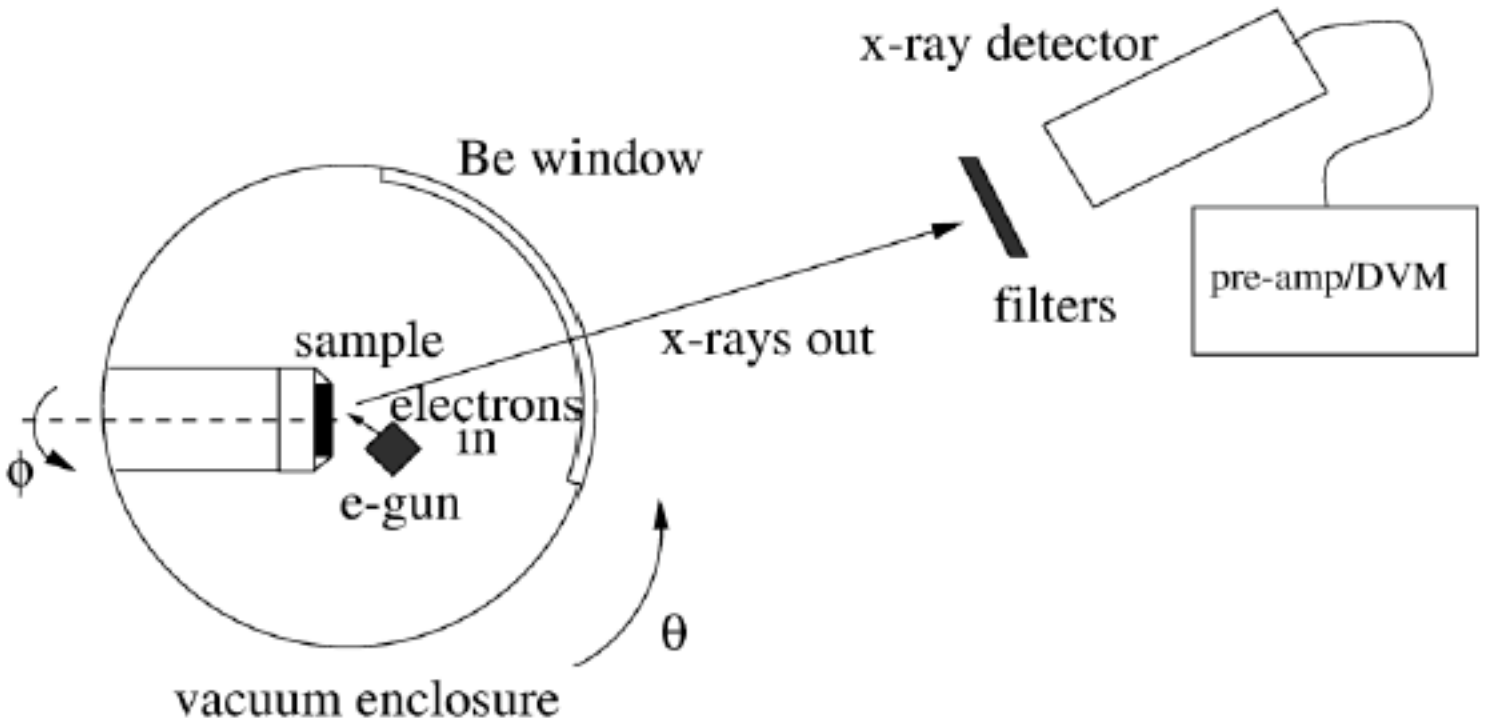


FIG. 1. Schematic of the x-ray holography experimental apparatus. The x rays produced inside the sample exit the vacuum chamber through a beryllium window. They are first energy filtered and then detected. The far-field hemisphere is measured by rotating the crystal 360° about its azimuthal axis $\phi$ and by rotating the vacuum chamber 90° about its polar axis $\theta$. The detectors remain fixed in space.

# Quantum electrodynamics of the internal source x-ray holographies: Bremsstrahlung, fluorescence, and multiple-energy x-ray holography

Gerald A. Miller and Larry B. Sorensen
*Department of Physics, University of Washington, Seattle, Washington 98195*
(Received 19 November 1996)

Quantum electrodynamics (QED) is used to derive the differential cross sections measured in the three new experimental internal source ensemble x-ray holographies: bremsstrahlung (BXH), fluorescence (XFH), and multiple-energy (MEXH) x-ray holography. The polarization dependence of the BXH cross section is also obtained. For BXH, we study analytically and numerically the possible effects of the virtual photons and electrons which enter QED calculations in summing over the intermediate states. For the low photon and electron energies used in the current experiments, we show that the virtual intermediate states produce only very small effects. This is because the uncertainty principle limits the distance that the virtual particles can propagate to be much shorter than the separation between the regions of high electron density in the adjacent atoms. We also find that using the asymptotic form of the scattering wave function causes about a 5–10 % error for near forward scattering. [S0163-1829(97)01622-6]

## I. INTRODUCTION

Fifty years ago, Gabor proposed electron holography as a method to improve the resolution of electron microscopes so that atoms could be directly imaged.[1] Gabor's idea was to focus the electron beam to a very small region of space just outside the sample to produce a nearly point source of radiation, and to record the interference pattern between the spherical reference wave from this point source and the spherical object waves produced when the electrons scattered from the atoms in the sample. This photographically recorded interference pattern would then be used as the diffraction grating in an optical reconstruction system. Although Gabor's dream to directly image atoms using holographic electron microscopy has never been realized (because the quality of the best electron lenses is only about as good as that of a raindrop for visible light[2]), Gabor's suggestion produced the optical holography revolution with the advent of lasers to provide the necessary coherent monochromatic external reference waves.

Ten years ago, Szöke pointed out that the necessary coherent spherical reference wave could also be created by generating the electron reference wave inside the sample.[3] In this case, the spatial coherence comes from the small spatial extent of the internal electron source. Szöke's internal source electron holography suggestion generated a flurry of activity,[4] and, in the past five years, Gabor's dream of directly imaging atoms with electrons has been partially realized for atoms within the first few atomic layers of the surface of a crystal using photoelectrons,[5] Auger electrons,[6] diffusely scattered low energy electrons,[7] and diffusely scattered Kikuchi electrons.[8] However, because electrons interact very strongly with atoms, the scattered object waves are not very good spherical waves (there is a strong angular variation of the magnitude and the phase of the electron-atom scattering amplitude), and multiple scattering produces ''electron focusing'' effects along the lines of atoms in the sample which are important. Consequently, these new electron holographies produce pictures of where the atoms are, but they do not accurately reconstruct the atomic positions. Szöke also proposed internal source x-ray holography using fluorescence x rays. Because x rays interact weakly with atoms, internal source x-ray holograms should produce much more accurate atomic resolution images than the internal source electron holographies.[9,10] Unfortunately, the price for this is that the modulation of the intensity in x-ray holograms $(1-5\times10^{-3})$ is about 100 times weaker than the modulation in electron holograms $(1-5\times10^{-1})$.

Earlier this year, the first atomic resolution x-ray holograms were produced using x-ray fluorescence holography[11] (XFH) and multiple-energy x-ray holography (MEXH).[12] About three years ago, stimulated by the advantages of multiple-energy electron holography[13] and the promise of XFH,[9] we started developing a new kind of internal source x-ray holography which uses bremsstrahlung photons created inside the sample.[14] The primary motivation for this paper is to provide the theoretical foundation for experimental bremsstrahlung x-ray holography (BXH) starting from quantum electrodynamics. The bulk of this paper is devoted to BXH, but we also show how the same quantum electrodynamic foundation applies to XFH and MEXH.

Bremsstrahlung x-ray holography is very attractive for three reasons: (1) Bremsstrahlung allows hard x rays to be produced from low $Z$ atoms. High quality holograms require the wavelength to be much smaller than the spacing between the atoms. The characteristic fluorescence energies of many interesting and important low $Z$ elements are too low to provide good images using XFH. (2) Bremsstrahlung produces x rays with a wide spread in their energy and allows multiple energy holograms to be recorded simultaneously by energy analyzing the bremsstrahlung photons. To accurately reconstruct a three-dimensional object in real space, we need information over a three-dimensional volume in reciprocal space. To overcome the problems in the internal source single-energy electron holographies, several multiple-energy methods have been developed.[13] These multiple-energy elec-

 

tron methods eliminate the twin images, greatly reduce the effects due to the strong angular variation of the magnitude and phase of the electron-atom scattering amplitude, and reduce the noise in the reconstructions. The MEXH method was developed in analogy to the multiple-energy electron methods to provide higher quality holograms than the single-energy XFH method. (3) The bremsstrahlung production cross section is extremely high. A conventional 400 W x-ray source produces about $10^{13}$ short wavelength bremsstrahlung photons per second into $4\pi$ steradians.[14] If all of these photons could be collected and energy analyzed, a very high quality BXH could be generated with a tabletop apparatus in a few hours.

The implementation of bremsstrahlung x-ray holography raises a number of interesting theoretical questions. We first recall that bremsstrahlung photons can have any energy from nearly zero to the energy of the incident electron, and the spectral intensity diverges at low energies: $I(\omega)d\omega \sim \omega^{-1}d\omega$. The bremsstrahlung photons, which scatter in the target crystal to produce the object waves, are intermediate or virtual particles. The momentum of each intermediate bremsstrahlung photon can take on any value; we must integrate over all virtual momenta in computing the scattering amplitude. Of course, this must occur for any intermediate particle that produces an object wave, but the possible problems are potentially more serious here for the virtual bremsstrahlung photons because of the broad nature of the bremsstrahlung spectrum.

More generally we should ask: Are quantum mechanical effects ever important in internal source x-ray holography? Or does the simple wave picture always work? If a quantum mechanical approach is needed, what is the correct quantum mechanical description of internal source x-ray holography? When can multipath photon interference be treated by the scalar wave equation approximation to Maxwell's equations instead of the full theory of quantum electrodynamics? To answer these questions, we develop a quantum electrodynamic treatment of the three internal source x-ray holographies, BXH, XFH, and MEXH, and compare it in detail with the simple wave picture.

It is useful to provide this connection between the fundamental theory (QED) and these new holographies. Almost all of the work in this field has been based on the simple wave picture. For example, Barton's original holographic inversion procedure[15] for electrons is based on the Helmholtz-Kirchoff inversion procedure for classical scalar waves. However, in the nonrelativistic limit, Rous and Rubin[16] have recently shown how the Lippmann-Schwinger equation can be used to provide solutions to the Schrödinger equation which correctly describe the physics of the single-energy electron internal source holographies.

For BXH in particular, classical electrodynamics will not produce the correct answer at high energies because the intermediate photons and electrons are virtual: the square of their four-momenta may not be equal to the square of their rest masses, $p^2 \neq m^2$. The physics can be divided into on-the-mass-shell amplitudes (called the ''on-shell'' or ''real'' processes) when $p^2 = m^2$, and off-the-mass-shell amplitudes (called ''off-shell'' or ''virtual'' processes) when $p^2 \neq m^2$. We show by explicit calculation that the virtual photons and virtual electrons do not propagate over the entire distance between the regions of high electron density in two adjacent atoms, and consequently classical electrodynamics predicts the right behavior. The reason for this comes from the uncertainty principle. The amount of off-shellness, or virtuality, of photons of energy $k_0$ and momentum $\vec{k}$ is measured by the quantity $k_0^2 - \vec{k}^2 \equiv Q^2$. If $k_0 > |\vec{k}|$, the virtual photon is not massless and its range is $Q^{-1}$ which is much smaller than the interatomic spacing $a$. If $k_0 < |\vec{k}|$, $Q^2$ is negative and $\exp(i|Q|r)$ oscillates rapidly for $r \sim a$ and any important contributions are cancelled.

Thus our main result is that for real atoms in real solids, excited to emit bremsstrahlung or fluorescence x-ray radiation, classical electrodynamics works very well because there is no significant overlap between the regions of high electron density in the adjacent atoms. However, because the intermediate state photons and electrons in the internal source x-ray holographies are virtual, it is important to use quantum electrodynamics to derive the equations necessary to analyze the holograms. We provide that derivation for BXH, XFH, and MEXH.

The separated atom approximation that we use to show that the full quantum electrodynamic treatment reduces to the classical electrodynamic expressions for real atoms in real solids, is formally analogous to the separated scatterer approximation used in analyzing high energy hadron-nuclear scattering experiments.[17–20]

Almost all of our knowledge of the atomic scale structure of bulk condensed matter has been determined from measurements of the quantum mechanical interference patterns that arise from particle-crystal scattering. How do the new x-ray holographies compare with crystallography, and what are the other possibilities? There are four equivalence classes of quantum mechanical interference patterns that have been used to determine structure: (1) In crystallography, there is an external source of particles which are sent into the crystal in nearly plane wave states. In the usual kinematic scattering limit, these particles coherently single scatter from many atoms in the crystal. The interference between these many single-scattering events produces the Bragg peaks.[21] (2) In internal source holography, there is an internal source of particles which leave the crystal in nearly spherical wave states. These particles coherently single scatter from the object atoms in the crystal. The interference between each of these single-scattering events and the strong direct path reference beam produces the Gabor zone plates in the hologram. (3) In external source holography, there is a coherent external source of particles which is sent into the crystal in nearly plane wave states. These particles coherently single scatter from the object atoms in the crystal. The interference between each of these single-scattering events and the strong reference beam produces the hologram. Unfortunately, the necessary coherent hard x-ray sources are not yet available[22] and when they become available they will probably destroy the sample in the process of making the hologram.[23] (4) In the Kichuchi and Kossel methods, there is an internal source of particles which leave the crystal in nearly spherical wave states. These particles coherently multiply scatter from many atoms in the crystal. The interference between these many multiple-scattering events produces the Kichuchi and Kossel patterns. These multiple-scattering patterns also contain use-

ful holographiclike information,[24] but this information is different than the single-scattering holograms.

The remainder of this paper is organized as follows. Section II outlines the standard classical scalar wave derivation of the intensity of the holographic interference pattern for the interference between a spherical reference wave and a spherical object wave. Section III is devoted to deriving an expression for the corresponding cross section for the intensity of the holographic interference pattern for bremsstrahlung holography. Since this paper is concerned with the possible effects of virtual photons, it is sufficient to consider the process as being bremsstrahlung production by the source atom followed by photon scattering by the object atom, located at a displacement $\vec{r}$ from the source atom. We find that we can simplify the expression for this cross section and apply it to holography if the atoms can be treated as well separated so that only real photons propagate from the source atom to the object atom. We then show for real atoms in real crystals that the regions of high electron density are sufficiently well separated. Our separated atom approximation is presented in Sec. IV. The bremsstrahlung energies for the experiments we are considering are 40–60 keV and at these energies, the x-ray-atom scattering cross section is dominated by the Thompson process. So we study the photon virtuality effects for bremsstrahlung production followed by Thomson scattering first. For this case, the corrections to our separated atom approximation are defined and shown to be entirely negligible in Sec. V. Near resonance, the anomalous scattering amplitude can become comparable to the Thompson scattering amplitude, and these two amplitudes interfere. We consider this case in Sec. VI, where we use the numerical results of the previous sections to justify the immediate use of the separated atom approximation. In XFH, the photon is produced by fluorescence radiation, where the excited atomic state is produced by electron or photon impact, and the atom decays via photon emission. The emitted photon can be scattered by another atom to produce an object amplitude which will interfere with the direct reference amplitude. This is discussed in Sec. VII, where the necessary amplitudes for this process are presented. In MEXH, a real photon is sent into the sample from outside. This photon has a direct path to the detector atom and a collection of single scattering paths to the detector atom via the object atoms which will interfere with the direct path. This is discussed in Sec. VIII. The final section is devoted to a brief summary and discussion.

## II. CLASSICAL INTERNAL SOURCE ENSEMBLE X-RAY HOLOGRAPHY

When an x-ray photon is created inside a solid and is detected outside, the quantum mechanical interference between the different paths that the photon takes as it leaves the solid will produce a holographic image of the atoms around the position where the photon is created. As we show below, the probability distribution for the photon intensity is a Gabor hologram. In contrast to the usual external source x-ray holography where the reference wave comes from outside the sample, in internal source x-ray holography, the wave corresponding to the direct amplitude (i.e., the amplitude for the photon to leave the solid without any interactions) serves as the reference wave, and the wave corresponding to the amplitude produced by single photon-atom scattering plays the role of the object wave.

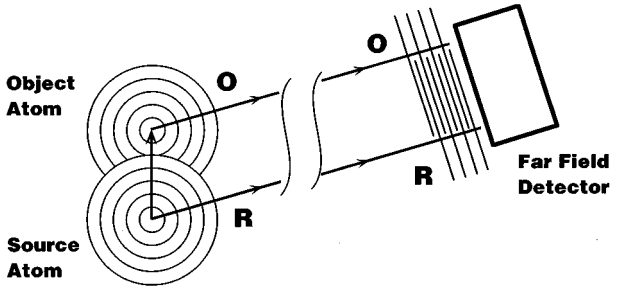


FIG. 1. The classical scalar wave description of internal source holography. The source atom produces the spherical reference wave $R$ which propagates directly to the detector, and which is scattered by the object atom to produce the spherical object wave $O$. The interference between $R$ and $O$ at the far field detector produces the internal source hologram.

Because the amplitude for photon-atom scattering is weak for hard x rays, the reference wave will be much stronger than the object waves, and this strong reference wave limit is the ideal holographic situation because the hologram is then dominated by the interference between the reference wave and the singly scattered object waves. In this limit, the interference between one object wave and another object wave, and the interference between the reference wave and the low order (double, triple, . . . ) multiple scattering object waves is much weaker than the interference between the reference wave and the single-scattering object waves. In nearly perfect crystals, the interference between the high order object waves can become comparable to the reference wave and is responsible for the Kossel (x-ray) and Kikuchi (electron) patterns. However, these multiple scattering features are sharp in angle and therefore can be easily removed from the hologram.

To develop the simple classical wave picture for internal source ensemble x-ray holography, consider first just the two atoms shown in Fig. 1. The full internal source x-ray hologram can be obtained from this two-atom case by summing over all object atoms for each source atom, and by summing over all source atoms. Suppose the source atom at the origin emits radiation which is detected in the far field, and suppose also that prior to detection the radiation is scattered by a second object atom located at position $\vec{a}$. The direct and single-scattering paths produce an interference pattern. When the polarization is not important, this problem can be treated as due to the interference between two scalar wave fields, with the scalar field representing a component of $\vec{E}$ or $\vec{B}$.

In this approximation, the first atom emits a scalar spherical reference wave $R$ of the form

$$R = \frac{e^{ikr}}{r}, \tag{1}$$

and the second atom emits a scalar spherical object wave $O$ of the form

$$O=\frac{e^{ika}}{a}f_a(\theta)\frac{e^{ik|\vec{r}-\vec{a}|}}{|\vec{r}-\vec{a}|}, \tag{2}$$

where again $\vec{a}$ is the position of the second atom. In the far field, $r\gg a$, the composite amplitude $M=R+O$ takes the form

$$M=\frac{e^{ikr}}{r}\left(1+e^{ika}\frac{f_a(\theta)}{a}e^{-i\vec{k}\cdot\vec{a}}\right), \tag{3}$$

where $f_a(\theta)$ is the standard atomic scattering amplitude for an incident plane wave, and we have followed the tradition in this field of neglecting the higher-order spherical wave corrections.

The far field intensity is given by the square of the composite amplitude $M$:

$$I=M^*M=R^*R+R^*O+RO^*+O^*O. \tag{4}$$

Holography records much more phase information than crystallography, but there is still a ''holographic phase problem'' present in the holographies that can only measure the intensity (e.g., laser, electron, and x-ray holography) and not the amplitude (e.g., acoustic and microwave holography). The intensity holographies record both the information we want about the object in the $R^*O$ term, and a copy of the complex conjugate of this information in the $RO^*$ term, which produces a nonexistent twin to the object during the reconstruction.

The far field object plus twin holographic interference cross term $R^*O+RO^*$ is proportional to

$$\mathrm{Re}[f_a(\theta)]\cos(ka-\vec{k}\cdot\vec{a})-\mathrm{Im}[f_a(\theta)]\sin(ka-\vec{k}\cdot\vec{a}). \tag{5}$$

In this paper, we treat the case in which the source atom emits x rays with wavelength $\lambda$. Note that to obtain significant holographic oscillations, it is important to make $\lambda\leqslant a$, and that the best holograms will be produced when $\lambda\ll a$.

Although all of the existing and proposed internal source holographic techniques actually depend on the multipath quantum mechanical interference of the particle emitted by the sample, the essential features of the holograms can be (and have been before this paper) obtained from the simple wave picture of the process outlined above.

There are two essential ingredients of atomic resolution internal source holography: (1) There is a localized source inside the sample. This localization provides the necessary spatial coherence of the source. The particle can be localized by being created inside the sample—this is the case for the bremsstrahlung and fluorescence x-ray holographies described in this paper. The particle can also be localized by being ejected from a specific quantum state in the sample—this is the case for photoelectron and Auger electron holography. In addition, the particle can be localized by an incoherent inelastic scattering event—this is the case for diffuse low energy electron diffraction (LEED) holography and diffuse Kikuchi electron holography. The analogous incoherent scattering localization is possible theoretically for photons via thermal diffuse x-ray scattering and via Compton scattering. (2) There is interference between the direct reference wave and the singly scattered object waves. This requires a coherent scattering event at the object atoms. If the object atoms scatter incoherently, the interference in the final state will not occur.

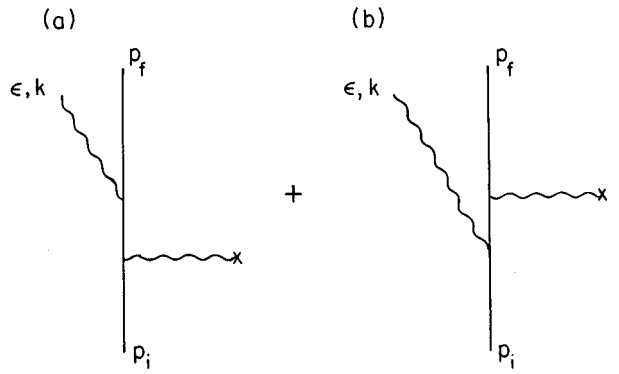


FIG. 2. The uncrossed (a) and crossed (b) Feynman diagrams for the reference amplitude $\mathcal{R}$ in bremsstrahlung x-ray holography (BXH). The $x$ represents the target atom that produces the bremsstrahlung photon. In the uncrossed (crossed) diagram, the outgoing photon is created after (before) the virtual photon is destroyed. The solid line represents the incident electron and the wiggly lines the photons; this standard convention is used in all the Feynman diagrams in this paper.

We shall show how these features arise from quantum electrodynamics.

## III. BREMSSTRAHLUNG X-RAY HOLOGRAPHY (BXH)

In the bremsstrahlung process, an electron incident on a solid radiates a photon: $e(p_i)+\mathrm{solid}\rightarrow e'(p_f)+\gamma(k)+\mathrm{solid}'$. In this paper, we consider the case where the initial and final electronic states of the atoms are the same, and where the solid is a collection of fixed atoms, i.e., we do not consider the effects of thermal motion. The Feynman diagrams for bremsstrahlung holography are shown in Figs. 2 and 3. The complete holographic amplitude $\mathcal{M}$ is the sum of the reference wave amplitude $\mathcal{R}$, given by the crossed and uncrossed Born bremsstrahlung terms shown in Fig. 2, and the object wave amplitude $\mathcal{O}$, given by the crossed and uncrossed Compton scattering terms shown in Fig. 3:

$$\mathcal{M}=\mathcal{R}+\mathcal{O}. \tag{6}$$

Here the QED reference $\mathcal{R}$, object $\mathcal{O}$, and hologram $\mathcal{M}$ amplitudes are analogous to the corresponding classical $R$, $O$, and $M$ terms in Eqs. (1)–(3). The quantum mechanical interference between $\mathcal{R}$ and $\mathcal{O}$ required to produce the holographic interference pattern $\mathcal{M}$, requires coherent scattering of the reference wave by the object atom. This required coherent Compton scattering by the single object atoms is provided by the recoiless Lamb-Mössbauer effect, in which the entire crystal lattice takes up the recoil momentum due to the Compton scattering. Consequently, the efficiency of this holographic process depends on the size of the recoiless fraction.

Before starting, it is useful to sketch the notational conventions used in this paper. The various four-momentum vectors are represented with italic typeface, e.g., $k, p_i, p_f$, and the three-vector spatial components are indicated with italic typeface with explicit arrows, e.g., $\vec{k}$, $\vec{p}_i$, and $\vec{p}_f$. The

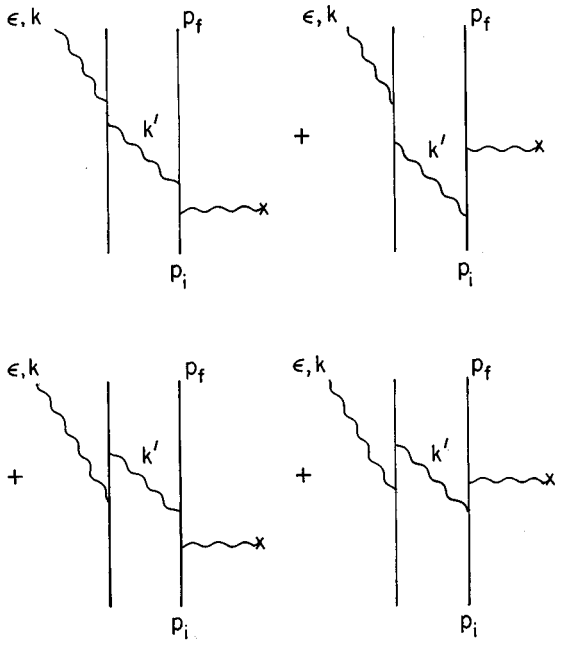


FIG. 3. The four Feynman diagrams for the BXH object amplitude $\mathcal{O}$. The object amplitude has four terms due to the crossed and uncrossed source terms, and the crossed and uncrossed Compton scattering terms. The sum of the two $\mathcal{R}$ diagrams in Fig. 2 interfere with the sum of the four $\mathcal{O}$ diagrams in this figure to produce the bremsstrahlung hologram.

magnitudes of three-vectors are written explicitly, e.g., $|\vec{k}|$. Thus for the bremsstrahlung reference amplitude shown in Fig. 2, the conservation of energy and momentum is written as $p_i+q=p_f+k$, where $\omega=k^0$, $p_i^0=E_i$, and $p_f^0=E_f$. Here $q$ is the four-momentum supplied by the target, $q=(0,\vec{q})$, where the 0 arises from our condition that no atoms (or nuclei) be excited. Three-momentum conservation is expressed as $\vec{q}+\vec{p}_i=\vec{p}_f+\vec{k}$. The notation and conventions of Bjorken and Drell[25] are used throughout the present work, and our units are such that both $\hbar$ and $c$ are unity.

The cross section for the holographic interference pattern is related to the square of the holographic amplitude $\mathcal{M}$ by

$$\frac{d^3\sigma}{d\Omega d\Omega_f d|\vec{k}|}=m^2\frac{p_f}{p_i}2\pi\frac{\omega\overline{|\mathcal{M}|^2}}{2(2\pi)^6}\theta(E_i-m-\omega), \tag{7}$$

where $m$ is the mass of the electron, $\Omega$ represents the outgoing angles of the photon and $\Omega_f$ those of the electron ($p_f$). The quantity $\overline{|\mathcal{M}^2|}$ is obtained from $|\mathcal{M}|^2$ by squaring the magnitude of $\mathcal{R}+\mathcal{O}$, summing over the spins of the final electron, and averaging over the spins of the initial electron.

The reference amplitude $\mathcal{R}$ shown diagrammatically in Fig. 2 is evaluated as

$$\mathcal{R}(k,q)=\frac{Ze_pe^2}{|\vec{q}|^2}\left[\bar{u}_f\left\{\left(\frac{\epsilon\cdot p_f}{2p_f\cdot k}-\frac{\epsilon\cdot p_i}{2p_i\cdot k}\right)\gamma^0+\frac{\not{\epsilon}\not{k}\gamma^0}{2p_f\cdot k}+\frac{\gamma^0\not{k}\not{\epsilon}\gamma^0}{2p_i\cdot k}\right\}u_i\right][1-F(|\vec{q}|)], \tag{8}$$

where $e^2/4\pi=\alpha$, the proton charge is the negative of the electron charge $e_p=-e$, and $F(|\vec{q}|)$ is the electronic contribution to the atomic form factor, normalized so that $F(0)=1$. This matrix element is proportional to $\epsilon_\mu=(0,\hat{\epsilon})$. The nuclear form factor is essentially unity for the kinematic range of the current x-ray holography experiments. The deviation of the term $[1-F(|\vec{q}|)]$ from unity represents the screening effect of the atomic electrons. If $\vec{q}=0$, the atom acts as a neutral object and there is no bremsstrahlung.

The only significant approximation made in obtaining Eq. (8) is that the initial and final state electron-nuclear Coulomb interactions have been neglected. The influence of these interactions, which can increase the value of the computed cross sections significantly, can be reasonably well approximated by multiplying the above amplitude by the product of the continuum electronic wave functions evaluated at the nuclear center—this is the Elwert approximation of Ref. 26. This is a well-motivated approximation classically because the acceleration that leads to the bremsstrahlung takes place in the vicinity of the nucleus. Detailed numerical studies[27] have confirmed the qualitative accuracy of the Elwert approximation. Multiplying our amplitude by this factor does not influence the propagation of the virtual photon between atoms, which is our principle concern. Thus we shall ignore the initial and final state interactions here in our study of the potential off-shell effects.

It is convenient to define the expressions in the bracket as $\epsilon\cdot B(k)$, so that the reference amplitude can be rewritten as

$$\mathcal{R}(k,q)=\frac{Ze_pe^2}{|\vec{q}|^2}[1-F(|\vec{q}|)]B_\mu(k)\epsilon^\mu. \tag{9}$$

As shown in Fig. 3, the virtual photon ($k'$) is produced by the source atom, propagates to the object atom, located at a separation $\vec{r}$ from the source, which scatters the virtual photon $k'$ so that the final photon $k$ is produced. The object atom scattering is dominated by the Compton scattering of the photon by the atomic electrons. This is because the photon-atom scattering is larger than the photon-nuclear scattering, by the ratio of the proton mass to the electron mass for the Thompson term, or by the ratio of the squares of the atomic and nuclear radii for the dipole terms. The virtual bremsstrahlung matrix element is denoted as $\tilde{B}_\mu(k')$ and the Compton rescattering transition matrix as $C^\mu(\epsilon,k,k')$. The evaluation of the Feynman graphs shown in Fig. 3 uses standard techniques.[25] Here we also carry out the integration over the time component of $k'$, which gives us a $\delta$ function setting $k'^0=\omega$. Then we arrive at the expression for the object amplitude:

$$\mathcal{O}=-Z^2e^4e_p\int\langle C^\mu(\epsilon,k,k')\rangle\frac{\tilde{B}_\mu(k')}{\omega^2-\vec{k}'^2+i\epsilon}\times e^{-i(\vec{k}-\vec{k}')\cdot\vec{r}}\frac{d^3k'}{(2\pi)^3}\frac{[1-F(|\vec{q}'|)]}{\vec{q}'^2+i\epsilon}, \tag{10}$$

where $\vec{q}'=\vec{p}_f-\vec{p}_i+\vec{k}'$. Note that $k'^2=\omega^2-\vec{k}'^2\neq 0$.

The bremsstrahlung matrix element is given by

$$\widetilde{B}_\mu(k')\equiv\bar{u}_f\left\{\gamma_0\,\frac{1}{\not p_i-\not k'+m}\,\gamma_\mu+\gamma_\mu\,\frac{1}{\not p_f+\not k'-m}\,\gamma_0\right\}u_i\,, \tag{11}$$

where standard spinor notation is used. Note that the Compton term $\langle C^\mu(\epsilon,k,k')\rangle$ is the atomic expectation value of the virtual-to-real Compton transition matrix which converts the virtual photon $k'$ to a real one with four-momentum and polarization $(k,\epsilon)$. Thus

$$C^\mu(\epsilon,k,k')=\gamma^\mu S_F(P_i-k)\not\epsilon+\not\epsilon S_F(P_f+k)\gamma^\mu, \tag{12}$$

where $S_F(P)$ is the relevant propagator for the bound electrons. For example, when the electrons are treated as free, the Compton transition matrix element is given by

$$C^\mu_{f,i}(\epsilon,k')\equiv\bar{U}_f\left\{\gamma^\mu\,\frac{1}{\not P_i-\not k-m}\,\not\epsilon+\not\epsilon\,\frac{1}{\not P_f+\not k-m}\,\gamma^\mu\right\}U_i\,, \tag{13}$$

where the upper case spinors $U_i\,,U_f$ represent the initial and final states of the free electron, with $\vec{P}_i+\vec{k}'=\vec{P}_f+\vec{k}$.

But the atomic bound states are more interesting. We may better understand the operator of Eq. (12) by noting that in the relativistic theory, the origin of the Thompson term comes from the terms involving the creation of virtual electron-antielectron pairs.[28] The resulting two-electron plus antielectron states live only for a very short time, so that we may ignore interactions with the other particles of the atom. The remaining terms can be seen in the nonrelativistic limit up to $\mathcal{O}(p^2/m^2)$ as arising from the two interactions of the dipole operator.[28] Then, we may write the Compton transition matrix element as a sum of terms so that

$$\langle C^\mu(\epsilon,k,k')\rangle=\langle T^\mu(\epsilon,k,k')\rangle+\langle R^\mu(\epsilon,k,k')\rangle, \tag{14}$$

where the Thompson scattering is denoted as $T^\mu(\epsilon,k,k')$ and the resonant scattering and other contributions are denoted as $\langle R^\mu(\epsilon,k,k')\rangle$.

When the long wavelength approximation is valid, we obtain

$$\langle R^\mu(\epsilon,k,k')\rangle=\omega^2e^2\sum_n\frac{\langle i|\hat{\epsilon}\cdot\vec{D}|n\rangle\langle n|D_l|i\rangle}{E_i+\omega-E_n+(1/2)i\Gamma_n}\delta_{\mu,l}+\omega^2e^2\sum_n\frac{\langle i|D_l|n\rangle\langle n|\hat{\epsilon}\cdot\vec{D}|i\rangle}{E_i-\omega-E_n}\delta_{\mu,l}\,, \tag{15}$$

where the dipole operator $\vec{D}$ is given by

$$\vec{D}=\sum_{i=1}^{Z}\vec{s}_i \tag{16}$$

and $\vec{s}_i$ is the displacement of the $i$th electron from the atomic center. The vector $\vec{D}$ is simply the sum of electronic dipole operators. The quantities $E_n$ and $\Gamma_n$ are the energy and the width of the excited state $n$. The result shown in Eq. (15) indicates that only the three-vector $\vec{R}$ part of $R^\mu$ enters into the expression for the amplitude. This is because each atomic photon emission and/or absorption is controlled by an $\hat{\epsilon}\cdot\vec{D}$ operator. For unpolarized atoms, $\vec{R}$ must be proportional to $\hat{\epsilon}$, so that it is convenient to define a strength function $S(\omega)$ such that

$$\vec{R}=\hat{\epsilon}S(\omega). \tag{17}$$

We use this definition along with Eq. (15) to obtain

$$S(\omega)=\omega^2e^2\sum_n|\langle i|\epsilon\cdot\vec{D}|n\rangle|^2\left[\frac{1}{E_i+\omega-E_n+(1/2)i\Gamma_n}+\frac{1}{E_i-\omega-E_n}\right]. \tag{18}$$

As noted in the Introduction, we shall proceed by first studying the effects of Thompson scattering by the object atoms. An explicit evaluation yields

$$\langle T^\mu\rangle=-\frac{1}{m}\delta^{\mu i}\epsilon_iF(|\vec{k}-\vec{k}'|), \tag{19}$$

where for simplicity we take the scattering object atom to be of the same type as the source atom which produced the virtual photon. In this and the following two sections we shall consider photons for which the Thompson term is dominant. We shall return to the resonant corrections to the Thompson term in Sec. V.

We compute $\overline{|\mathcal{M}^2|}$ by squaring $\mathcal{R}+\mathcal{O}$, keeping only the Thompson scattering contribution $T^\mu$ in $\mathcal{O}$, by summing over the final electron spin, and by averaging over the initial electron spin. The result is

$$\overline{|\mathcal{M}^2|}=\frac{1}{2}\sum_{s_fs_i}\left[B^*\cdot\epsilon B\cdot\epsilon\left(\frac{Ze^3}{|\vec{q}|^2}[1-F(|\vec{q}|)]\right)^2+\frac{Z^3e^8}{|\vec{q}|^2}[1-F(|\vec{q}|)]\times2\mathrm{Re}\left\{B^*(k)\cdot\epsilon\int\frac{d^3k'}{(2\pi)^3}\frac{[1-F(|\vec{q}'|)]}{|\vec{q}|'^2}e^{-i(\vec{k}-\vec{k}')\cdot\vec{r}}\frac{F(|\vec{k}-\vec{k}'|)}{\omega^2-\vec{k}'^2+i\epsilon}\langle T^\mu(\epsilon,k,k')\rangle\widetilde{B}_\mu(k')\right\}\right]. \tag{20}$$

Here the term of order $Z^4e^{10}$, which is much smaller than the lower-order terms, has been neglected.

The result given by Eq. (20), as specified by the matrix elements given by Eqs. (11) and (19), is our main result. It gives the bremsstrahlung holography cross section when the object scattering is dominated by the Thompson term. We shall make a further simplification to facilitate a first evaluation: we will keep only the numerically most significant terms of $B$ and $\widetilde{B}$, i.e., the ones proportional to $\hat{\epsilon}\cdot\vec{p}_f$ and $\hat{\epsilon}\cdot\vec{p}_i$. This leads to the standard classical expression for the bremsstrahlung cross section.[29] We have explicitly evaluated the neglected terms numerically and found that their neglect produces an approximately constant 10% reduction in the cross section over the kinematic region where the bremsstrahlung holography experiments will operate. Our numerical results can be understood by noting that $\not{\epsilon}\not{k}\gamma^0\approx i\vec{\sigma}\cdot\vec{\epsilon}\times\vec{k}$. This spin-dependent interaction is a magnetic effect proportional to $\vec{\nabla}\times\vec{A}$, which therefore does not interfere with the terms we keep. Furthermore, the two spin-dependent terms of Eq. (8) partially cancel and their sum is smaller than the leading term by about $k/m$.

We carry out the average over electron initial spin, and the sum over final electron spin. The result for the bremsstrahlung holography cross section is

$$\frac{d^3\sigma}{d\Omega\Omega_f|\vec{k}|}=m^2\,\frac{|\vec{p}_f|}{|\vec{p}_i|}\,\frac{1}{2}\,\frac{\omega}{(2\pi)^5}\,\theta(E_i-m-\omega)\overline{|\mathcal{M}|^2}\,\frac{1}{8m^2}\,[8E_iE_f-4p_i\cdot p_f+4m^2], \tag{21}$$

where

$$\overline{|\mathcal{M}|^2}\equiv\left(\frac{Ze^3}{|\vec{q}|^2}\,[1-F(|\vec{p}_f-\vec{p}_i+\vec{k}|)]\right)^2[\hat{\epsilon}\cdot\vec{V}(k)\hat{\epsilon}\cdot\vec{V}(k)]\,\frac{Z^3e^8}{|\vec{q}|^2}\,\frac{2[1-F(|\vec{q}|)]}{m}\,\mathrm{Re}I(\vec{k},\vec{r}). \tag{22}$$

Here the quantity $I(\vec{k},\vec{r})$ is given by

$$I(\vec{k},\vec{r})\equiv\hat{\epsilon}\cdot\vec{V}(k)\int\frac{d^3k'}{(2\pi)^3}\,\hat{\epsilon}\cdot\vec{V}_1(k')e^{-i(\vec{k}-\vec{k}')\cdot\vec{r}}\left(\frac{[1-F(|\vec{q}'|)]}{|\vec{q}'|^2}\,\frac{F(|\vec{k}-\vec{k}'|)}{\omega^2-\vec{k}'^2+i\epsilon}\right), \tag{23}$$

where $\vec{q}'=\vec{p}_f-\vec{p}_i+\vec{k}'$ and $\vec{q}=\vec{p}_f-\vec{p}_i+\vec{k}$. The vectors $\vec{V}(k)$ and $\vec{V}_1(k')$ are given by

$$\vec{V}(k)\equiv\frac{\vec{p}_f}{p_f\cdot k}-\frac{\vec{p}_i}{p_i\cdot k}, \tag{24}$$

$$\vec{V}_1(k')\equiv\frac{2\vec{p}_f}{2p_f\cdot k'+k'^2}-\frac{2\vec{p}_i}{2p_i\cdot k'-k'^2}. \tag{25}$$

The cross section for the intensity of a bremsstrahlung hologram given by Eq. (21) together with the definitions given by Eqs. (22)–(25) is the complete solution to the bremsstrahlung holography problem. What remains to be done is to carefully analyze these equations to see how the classical holography equations emerge in the classical limit, and to see how large the quantum effects are, and when they are important. That is the content of the next three sections.

## IV. SEPARATED ATOM APPROXIMATION

The goal of the bremsstrahlung holography experiments is to determine precise information about the location of the object atoms, which is represented in Eqs. (21)–(25) by the vector $\vec{r}$. The standard holography expressions involve an interference term of the general form $\beta e^{i\omega r}e^{-i\vec{k}\cdot\vec{r}}/r$ where $\beta$ is a known function. A quick look at Eqs. (22) and (23) could lead one to dismay. How could that integral ever have the simple form required for holographic investigations? We indicate a solution by considering the situation when the two atoms are very far apart, i.e., in the limit where $r$ approaches infinity. Here our intuition provides a guide: the process must proceed by bremsstrahlung from the source atom followed by photon propagation along the direction of $\vec{r}$ and Thompson scattering by the object atom. Thus the bremsstrahlung makes a real photon with momentum $\vec{\kappa}\equiv\omega\hat{r}$ and energy $\omega$, and the Thompson scattering changes the direction of $\vec{\kappa}$ to $\vec{k}$.

In this case, the photon has four momentum $\kappa\equiv(\omega,\vec{\kappa})$ and $\kappa\cdot\kappa=0$. The propagating photon is on shell. This situation is simple, but the full integral of Eq. (23) is not. However, we will evaluate this integral by developing expansions in which the leading term is correct in the limit that $r$ is very large. We shall keep the leading term and the most important corrections. We call this approach the separated atom approximation. In practice, this amounts to replacing $k'$ by $\kappa$ in certain terms in the integrand. For example, we shall show below that replacing $\vec{V}(k')$ by $\vec{V}(\kappa)$ and $\vec{q}'$ by $\vec{p}_f-\vec{p}_i+\vec{\kappa}$ are excellent approximations.

We may use the uncertainty principle to better understand why the propagating photon must be real for infinite values of $r$. Our virtual photons have energy $\omega$, but the magnitude of the three-momentum varies from 0 to infinity in the integration. Let us define $Q^2\equiv\omega^2-|\vec{k}'|^2$ to provide a measure of the violation of energy conservation required to make the virtual photon. This is simply the square of the energy-momentum four vector, which vanishes for real photons. If $Q^2<0$ the wave is a decaying exponential of the form $e^{-|\hbar Qr|}/r$, which has a small value. The interpretation of this Yukawa form is that the photon lives for a time $\hbar/Q$, so that its maximum range is $\hbar c/Q$. If $Q^2>0$, the wave is of the form $e^{i\hbar Qr}/r$. The effect of this term is very small because of

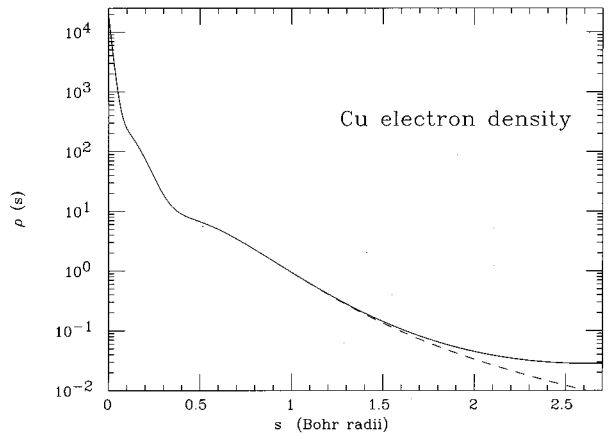


FIG. 4. The electron density $\rho(s)$ for isolated copper atoms (dashed line) and for copper atoms in crystalline copper (solid line) calculated using the FEFF computer code (Ref. 30). Here $s$ is the distance from the center of the atom.

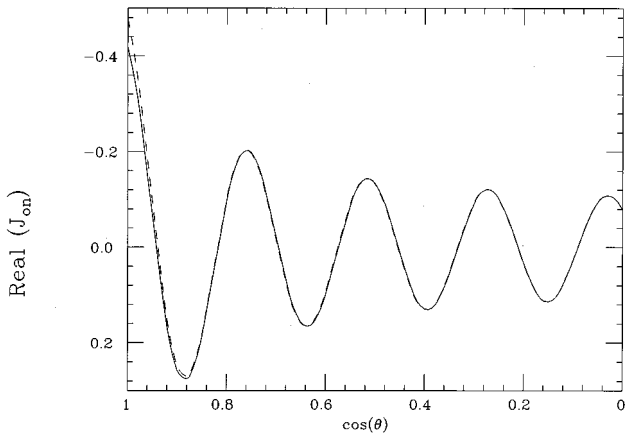


FIG. 5. Comparison of the real part of the on-shell separated atom approximation $J_{\rm on}$ (solid line) given by Eq. (27) with the real part of the classical spherical wave holography function (dashed line) given by Eq. (30). The results in Figs. 5–9 are shown for crystalline copper with representative experimental kinematics: the incident electron energy is 60 keV and the outgoing photon energy is 20 keV. Here $\cos(\theta)=\hat{k}\cdot\hat{r}$.

the oscillations of the integrand in the integral over $d^3k'$. Thus, the net result is that only the real photons with $Q=0$ reach the object atom.

Are the atoms in a real solid sufficiently separated so that all the virtual photon effects are gone before the bremsstrahlung photon reaches the nearest atoms? We argue that the answer is yes, at least for most solids at typical experimental bremsstrahlung holography energies, by considering the specific example of crystalline copper. In crystalline copper the atoms are separated by a distance $R_N\approx 2.5561$ Å$\approx 4.83a_0$ where $a_0$ is the Bohr radius $\sim 0.529$ Å. Where are the electrons in each atom? The electron density for isolated copper atoms and for crystalline copper calculated using the FEFF computer code[30] is shown in Fig. 4. Note that this density is sharply peaked at small values of $s$ since most of the electrons are within 1 Å of the nuclear center of the atom, and that the electron densities for isolated atoms and for atoms embedded in the solid are very similar. In particular, the root mean square radius of the displayed density is $1.08a_0$. Thus the closest separation $r$ between the copper atoms is about 5 times the typical value of the distance $s$ between an electron and the nucleus. At the very least, it is reasonable to expect that the separated atom approximation is a good starting point.

Our procedure is to examine a set of approximations to the full results for $I(\vec{k},\vec{r})$ given by Eq. (23). We will define the on-shell, separated atom approximation as the result of setting $\vec{k}'=\vec{\kappa}$ in $V_1(k')$ and in $\vec{q}'$. Then the on-shell approximation $I_{\rm on}(\vec{k},\vec{r})$ to the full on- and off-shell integral $I(\vec{k},\vec{r})$ is given by

$$I_{\rm on}(\vec{k},\vec{r})=\frac{[1-F(|\vec{p}_f-\vec{p}_i+\vec{\kappa}|)][1-F(|\vec{q}|)]}{|\vec{p}_f-\vec{p}_i+\vec{\kappa}|^2}\times\hat{\epsilon}\cdot\vec{V}(k)\,\hat{\epsilon}\cdot\vec{V}(\kappa)J_{\rm on}(\vec{k},\vec{r}),\tag{26}$$

where

$$J_{\rm on}(\vec{k},\vec{r})=\int\frac{d^3k'}{(2\pi)^3}e^{-i(\vec{k}-\vec{k}')\cdot\vec{r}}\frac{F(|\vec{k}-\vec{k}'|)}{\omega^2-\vec{k}'^2+i\epsilon}.\tag{27}$$

Again, the subscript ''on'' is to remind us that setting $\vec{k}'$ equal to $\vec{\kappa}$ causes the propagating photon to be on shell. Its virtuality has decayed by the time it reaches the near-neighbor atoms, and the square of its four momentum has vanished. The next section (Sec. V) is devoted to the demonstration that the on-shell $I_{\rm on}(\vec{k},\vec{r})$ given by Eq. (26) is an excellent approximation to the full $I(\vec{k},\vec{r})$ given by Eq. (23).

The first step is to understand the integral $J_{\rm on}$. We can gain some insight by converting the integral over the momentum into one involving positions. We use

$$F(|\vec{k}-\vec{k}'|)\equiv\int d^3s\rho(s)e^{-i(\vec{k}-\vec{k}')\cdot\vec{s}},\tag{28}$$

so that the on-shell $J_{\rm on}$ integral given in Eq. (27) simplifies to

$$J_{\rm on}(\vec{k},\vec{r})=-\frac{1}{4\pi}\int d^3s\rho(s)\frac{e^{i\omega|\vec{s}+\vec{r}|}}{|\vec{s}+\vec{r}|}e^{-i\vec{k}\cdot(\vec{s}+\vec{r})}.\tag{29}$$

If $r\gg s$ for the important regions of $\rho(s)$, we may replace $e^{i\omega|\vec{s}+\vec{r}|}/|\vec{s}+\vec{r}|$ by $e^{i\omega r}e^{i\omega\vec{r}\cdot\vec{s}}/r$. This gives

$$\lim_{r\to\infty}J_{\rm on}(\vec{k},\vec{r})=-\frac{1}{4\pi}\frac{e^{i\omega r}}{r}e^{-i\vec{k}\cdot\vec{r}}F(|\vec{k}-\vec{\kappa}|),\tag{30}$$

which has the usual classical holographic form. The spherical Green's function $e^{i\omega r}/r$ corresponds to the form of the wave at infinity. This form arises from the pole in the integral for $J_{\rm on}$ at $|\vec{k}'|=\omega$.

To check the asymptotic approximation given in Eq. (30) we numerically compared the full $J_{\rm on}$ given by Eq. (29) with its approximation given by Eq. (30). The results are shown in Fig. 5. Note that the approximation is excellent except when $\vec{k}\|\vec{r}$. Even then, the full theory and the approximation produce very similar holographic interference patterns; the asymptotic approximation produces a pattern about 10% smaller than the full theory when $\vec{k}\|\vec{r}$. This agreement be-

tween the full quantum electrodynamic calculation and the simple classical holography equations shows that bremsstrahlung holography is possible: the reduction for $\vec{k}\|\vec{r}$ does not significantly change the oscillatory form with its strong dependence on $\vec{k}\cdot\vec{r}$.

There is no need to use the asymptotic approximation in numerical work. We may use the correct value of $J_{\rm on}$ and maintain the explicit holographic form. This involves expanding the form factor in terms of Legendre polynomials $P_L(\hat{k}\cdot\hat{k}')$:

$$F(|\vec{k}-\vec{k}'|)=\sum_L F_L(\omega r)P_L(\hat{k}\cdot\hat{k}'), \tag{31}$$

where $\omega=|\vec{k}|$. Combining the partial wave expansion for the atomic form factor given by Eq. (31) with the full expression for $J_{\rm on}$ given by Eq. (27) yields the partial wave expression for $J_{\rm on}$

$$J_{\rm on}(\vec{k},\vec{r})=i\omega\sum_L i^L F_L(\omega r)h_L^{(1)}(\omega r)P_L(\hat{k}\cdot\hat{r}), \tag{32}$$

where $h_L^{(1)}(\omega r)$ are the outgoing spherical Bessel functions. All that is required for this to hold is that $r$ be bigger than the maximum value of $s$ (i.e., *circa* 2.56 Å for copper) occurring in the integral (29). Since $r=2.56$ Å and Fig. 4 shows that $\rho(s)$ is less than $10^{-3}$ of its maximum value for $s\geq 0.5$ Å, this condition is met. We may also understand the relation between this expression and its limiting form shown in Eq. (30). The use of the asymptotic form of the outgoing spherical Bessel functions:

$$\lim_{x\to\infty} h_L^{(1)}(x)=(-i)^{L+1}\frac{e^{ix}}{x}, \tag{33}$$

leads immediately to the result shown in Eq. (30). The corrections to this asymptotic form are thus of order $1/x$ times the original result. Thus we see that the expected first correction to Eq. (30) is of the order of $1/\omega r\approx 1/25$ for $\omega=20$ keV.

Equation (32) allows us to understand why the difference between the asymptotic approximation given by Eq. (30) and the exact result given by Eq. (32) is largest for $\vec{k}\cdot\vec{r}=1$. The terms $F_L(\omega r)h_L(\omega r)$ monotonically approach zero as $L$ increases. The function $P_L(\vec{k}\cdot\vec{r}=1)=1$ for all $L$, so that the terms with large $L$ [these are the terms for which the approximation generated by Eq. (33) is less accurate] add constructively. This can also be seen (without using the partial wave expansion) by examining the integrand of Eq. (29). If $\hat{k}\cdot\hat{r}=1$ (i.e., when $\vec{k}\|\vec{r}$), the term $\omega|\vec{s}+\vec{r}|-\vec{k}\cdot\vec{s}$ is greatly reduced so that the contributions of the larger values of s are less inhibited by the oscillating exponential than for other values of $\vec{k}\cdot\vec{r}$.

The partial wave expression (32) systematically gives all of the corrections to the classical holographic form given by Eq. (30). However, it is useful to provide another approximation which shows us why the relevant integrals are dominated by terms in which $\vec{k}'=\vec{\kappa}$. The idea is to approximate $F(|\vec{k}-\vec{k}'|)$ using

$$F(|\vec{k}-\vec{k}'|)\approx F(q_1)+(\vec{k}'-\vec{\kappa})\cdot\vec{\nabla}_{q_1}F(q_1), \tag{34}$$

where $q_1\equiv|\vec{k}-\vec{\kappa}|$. We use Eq. (34) in the integral (27) and note that the $\vec{k}'$ appearing in the numerator of the integral (26) can be replaced by a gradient on $\vec{r}$. Thus we find

$$J_{\rm on}(\vec{k},\vec{r})\approx -\frac{1}{4\pi}\frac{e^{i\omega r}}{r}e^{-i\vec{\kappa}\cdot\vec{r}}F(q_1)+\delta J_{\rm on}, \tag{35}$$

with

$$\delta J_{\rm on}(\vec{k},\vec{r})\equiv -e^{-i\vec{\kappa}\cdot\vec{r}}\vec{\nabla}_{q_1}F(q_1)\cdot\vec{V}_{\rm on}(\vec{k},\vec{r}), \tag{36}$$

where

$$\vec{V}_{\rm on}(\vec{k},\vec{r})\equiv\left(\frac{\vec{\nabla}_r}{i}-\vec{\kappa}\right)\int\frac{d^3k'}{(2\pi)^3}e^{i\vec{k}'\cdot\vec{r}}\left\{\frac{F(|\vec{k}-\vec{k}'|)}{\omega^2-\vec{k}'^2+i\epsilon}\right\}. \tag{37}$$

One may use the Legendre partial wave expansion of Eq. (32) above to obtain a more detailed expression for $\vec{V}_{\rm on}(\vec{k},\vec{r})$. But the main point is that the long distance behavior of the integral is that of $e^{i\omega r}$. Since $(-i\vec{\nabla}_r-\vec{\kappa})e^{i\omega r}=0$, the correction to the separated atom approximation must have an extra factor of order $1/\omega r\approx 1/25$. We shall use expansions similar to that of Eq. (34) to systematically understand the short distance terms. The integral $\vec{V}_{\rm on}(\vec{k},\vec{r})$ will appear again. Furthermore, we shall often employ the technique of writing a complete expression as its on-shell approximation plus a term which is proportional to $(-i\vec{\nabla}_r-\vec{\kappa})$ and vanishes in the asymptotic limit given by Eq. (30).

## V. SHORT RANGE TERMS

In the previous section we showed how keeping the effects of the pole at $|\vec{k}'|=\omega$ led to the term with the long distance propagation. Here we show that this pole dominates the complete expression given by Eq. (23). The vector $\vec{k}'$ appears in three places in this integral, in $[1-F(|\vec{q}'|)]$, in $1/|\vec{q}'|^2$, and in $\vec{V}_1(k')$. We will denote these terms as the screening correction, the Coulomb photon propagation, and the electron propagation. We shall study each one separately.

### A. Screening correction

Keeping the $\vec{k}'$ in the screening term leads to the integral, $I_s$:

$$I_s(\vec{k},\vec{r})=\int\frac{d^3k'}{(2\pi)^3}e^{-i(\vec{k}-\vec{k}')\cdot\vec{r}}\left\{[1-F(|\vec{q}'|)]\frac{F(|\vec{k}-\vec{k}'|)}{\omega^2-\vec{k}'^2+i\epsilon}\right\}. \tag{38}$$

Recall that $\vec{q}'=\vec{p}_f-\vec{p}_i+\vec{k}'$. Pole dominance of the integral would allow us to replace the $\vec{k}'$ appearing in $\vec{q}'$ by $\vec{\kappa}$. Thus the integral may be approximated by using

$$\begin{aligned}F(|\vec{q}'|)&=F[|\vec{p}_f-\vec{p}_i+\vec{\kappa}+(\vec{k}'-\vec{\kappa})|]\\&\approx F(|\vec{p}_f-\vec{p}_i+\vec{\kappa}|)+(\vec{k}'-\vec{\kappa})\cdot\vec{\nabla}_{q_2}F(q_2),\end{aligned} \tag{39}$$

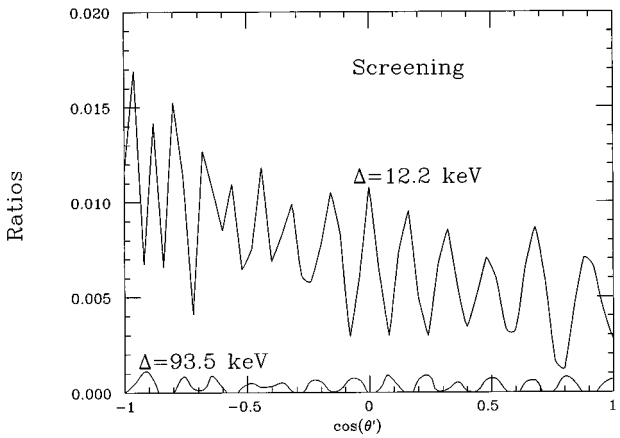


FIG. 6. The small effects of photon virtuality on the screening correction given by the ratio of the second to the first term in Eq. (40). The ratio $\mathrm{Re}\delta I_s/\mathrm{Re}\{[1-F(q_2)]J_{\mathrm{on}}\}$ is plotted to illustrate the size of these corrections for two typical experimental values of the momentum transfer, namely 12.2 keV and 93.5 keV. Here the momentum transfer $\vec{\Delta}\equiv\vec{p}_i-\vec{p}_f$ and the angle $\theta'$ is specified by $\cos(\theta')=\hat{\Delta}\cdot\hat{r}$.

where $q_2=|\vec{p}_f-\vec{p}_i+\vec{\kappa}|$. Using this in Eq. (38) leads to the appearance of $\vec{k}'$ in the numerator of the integral, which can again be replaced by a gradient on $\vec{r}$. The result is

$$I_s(\vec{k},\vec{r})\approx[1-F(q_2)]J_{\mathrm{on}}(\vec{k},\vec{r})+\delta I_s(\vec{k},\vec{r}) \tag{40}$$

with

$$\delta I_s(\vec{k},\vec{r})\equiv -e^{-i\vec{k}\cdot\vec{r}}\vec{\nabla}_{q_2}F(q_2)\cdot\vec{V}_{\mathrm{on}}(\vec{k},\vec{r}). \tag{41}$$

The leading long distance behavior of the integral of Eq. (37) required to evaluate $\vec{V}_{\mathrm{on}}$ is that of $e^{i\omega r}$. But $(-i\vec{\nabla}_r-\vec{\kappa})e^{i\omega r}=0$. Furthermore, $\vec{\nabla}_{q_2}F(q_2)$ is of order $(n/q_2)F(q_2)$, with $n\approx 4$. Thus, the $\delta I_s(\vec{k},\vec{r})$ screening correction term of Eq. (40) provides a correction which has an extra factor of $F(q_2)/q_2 r$ compared to the leading term. However, $F(q_2)$ is very small, 1% at most, for the kinematics of this experiment. For typical kinematics $q_2\approx 100$ keV so $(n/q_2 r)F(q_2)\approx(4/125)(1/100)\approx 3\times 10^{-4}$. The correction to the separated atom approximation due to the screening term is completely negligible here. This is shown in Fig. 6.

### B. Coulomb photon propagation

If we keep the $\vec{k}'$ in the Coulomb photon propagator $1/|\vec{q}'|^2$, we need to evaluate the Coulomb integral $I_{\mathrm{Coul}}(\vec{k},\vec{r})$:

$$I_{\mathrm{Coul}}(\vec{k},\vec{r}) = \int\frac{d^3k'}{(2\pi)^3}e^{-i(\vec{k}-\vec{k}')\cdot\vec{r}}\left\{\frac{1}{|\vec{p}_f-\vec{p}_i+\vec{k}'|^2}\frac{F(|\vec{k}-\vec{k}'|)}{\omega^2-\vec{k}'^2+i\epsilon}\right\}. \tag{42}$$

In this case, there are two sets of poles. One is the usual one at $|\vec{k}'|=\omega$, but there is also a set of poles off the real axis (in the complex $|\vec{k}'|$ plane) corresponding to the zeros of $|\vec{p}_f-\vec{p}_i+\vec{k}'|^2$. It is desirable to handle these pole terms separately, so we use the identity

$$\frac{1}{A}\cdot\frac{1}{B}\equiv\left[\frac{1}{A}+\frac{1}{B}\right]\frac{1}{A+B} \tag{43}$$

in the form

$$\frac{1}{|\vec{p}_f-\vec{p}_i+\vec{k}'|^2}\cdot\frac{1}{\omega^2-\vec{k}'^2+i\epsilon} =\left[\frac{1}{\omega^2-\vec{k}'^2+i\epsilon}+\frac{1}{|\vec{p}_f-\vec{p}_i+\vec{k}'|^2}\right] \times\frac{1}{\omega^2+(\vec{p}_i-\vec{p}_f)^2+2\vec{k}'\cdot(\vec{p}_f-\vec{p}_i)}. \tag{44}$$

The first term has the pole at $|\vec{k}'|=\omega$ which is responsible for the long distance photon propagation. The second term has the above-mentioned poles of $|\vec{k}'|$ off the real axis. The vanishing of the denominator $\omega^2+(\vec{p}_i-\vec{p}_f)^2+2\vec{k}'\cdot(\vec{p}_f-\vec{p}_i)$ occurs only when the two terms in the bracket cancel and causes no mathematical difficulty. The first term of Eq. (44) can be approximated by using $\vec{k}'=\vec{\kappa}+(\vec{k}'-\vec{\kappa})$ and expanding so that

$$\frac{1}{\omega^2-\vec{k}'^2+i\epsilon}\cdot\frac{1}{\omega^2+(\vec{p}_i-\vec{p}_f)^2+2\vec{k}'\cdot(\vec{p}_f-\vec{p}_i)} \approx\frac{1}{\omega^2-\vec{k}'^2+i\epsilon}\frac{1}{(\vec{p}_f-\vec{p}_i+\vec{\kappa})^2}\left[1-\frac{2(\vec{k}'-\vec{\kappa})\cdot(\vec{p}_f-\vec{p}_i)}{(\vec{p}_f-\vec{p}_i+\kappa)^2}\right]. \tag{45}$$

The first part of Eq. (45) corresponds to the separated atom approximation. The next term involves $(\vec{k}'-\vec{\kappa})$ which yields the integral $V_{\mathrm{on}}(\vec{k},\vec{r})$ of Eq. (37). The specific correction to $J_{\mathrm{on}}$ is denoted as $\delta J_{\mathrm{on}}^{\mathrm{Coul}}$ which is obtained by keeping the second term of Eq. (45) in the $I_c$ integral given by Eq. (38) so that

$$\delta J_{\mathrm{on}}^{\mathrm{Coul}}(\vec{k},\vec{r}) \equiv(-2)\int\frac{d^3k'}{(2\pi)^3}e^{-i(\vec{k}-\vec{k}')\cdot\vec{r}}\left\{\frac{(\vec{k}'-\vec{\kappa})\cdot(\vec{p}_f-\vec{p}_i)}{\omega^2-\vec{k}'^2+i\epsilon}\right\}. \tag{46}$$

The $\vec{k}'-\vec{\kappa}$ term of Eq. (46) again leads to an extra factor of $1/q_2 r$, as compared to the leading term. The expected small size of this correction is confirmed by numerical evaluation. Indeed the second term of Eq. (45) is negligible except for the angles for which the leading term vanishes. See Fig. 7, which shows the relative sizes of $J_{\mathrm{on}}(\vec{k},\vec{r})/(\vec{p}_f-\vec{p}_i+\vec{\kappa})^2$ and the correction to it due to $\delta J_{\mathrm{on}}^{\mathrm{Coul}}(\vec{k},\vec{r})/(\vec{p}_f-\vec{p}_i+\vec{\kappa})^2$.

What about the second term of Eq. (44)? This is given by

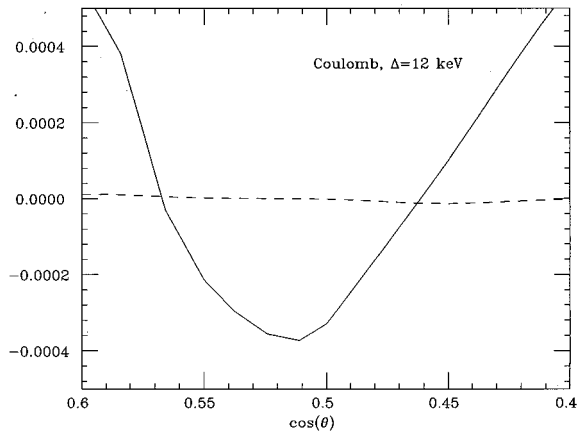


FIG. 7. The small effects of virtual photon propagation on the Coulomb correction. The real part of the on-shell Coulomb correction $\delta J_{\rm on}^{\rm coul}/(\vec{p}_f-\vec{p}_i+\vec{\kappa})^2$ (dashed line) given by Eq. (46) is compared with the real part of the full on-shell separated atom approximation $J_{\rm on}/(\vec{p}_f-\vec{p}_i+\vec{\kappa})^2$ (solid line) given by Eq. (27). Here $\Delta=12$ keV, $\hat{p}_i\cdot\hat{r}=0.5$, and $\hat{p}_f\cdot\hat{p}_1=0.5$.

$$\left[\frac{1}{|\vec{p}_f-\vec{p}_i+\vec{k}'|^2}\right]\frac{1}{\omega^2+(\vec{p}_i-\vec{p}_f)^2+2\vec{k}'\cdot(\vec{p}_f-\vec{p}_i)}.$$

It is necessary to treat the $\vec{k}'\cdot\vec{k}'$ terms correctly, but the term $\vec{k}'\cdot(\vec{p}_f-\vec{p}_i)$ may be evaluated by using $\vec{k}'=\vec{\kappa}+(\vec{k}'-\vec{\kappa})$ and treating the difference term as a perturbation in $\vec{k}'-\vec{\kappa}$. Thus

$$\frac{1}{|\vec{p}_f-\vec{p}_i+\vec{k}'|^2}\approx\frac{1}{(\vec{p}_f-\vec{p}_i)^2+2\vec{\kappa}\cdot(\vec{p}_f-\vec{p}_i)+\vec{k}'\cdot\vec{k}'}-\frac{2(\vec{k}'-\vec{\kappa})\cdot(\vec{p}_f-\vec{p}_i)}{[(\vec{p}_f-\vec{p}_i)^2+2\vec{\kappa}\cdot(\vec{p}_f-\vec{p}_i)+\vec{k}'\cdot\vec{k}']^2}. \tag{47}$$

If we treat this as a function of $|\vec{k}'|$, the poles in the exact expression and in its approximation given by the first term, appear at the same positions. The second term can be thought of as correcting the value of the residue at the pole. Furthermore, it vanishes for well-separated atoms. Thus neglecting the second term is a good approximation. We use similar logic to write

$$\frac{1}{\omega^2+(\vec{p}_i-\vec{p}_f)^2+2\vec{k}'\cdot(\vec{p}_f-\vec{p}_i)}\approx\frac{1}{\omega^2+(\vec{p}_i-\vec{p}_f)^2+2\vec{\kappa}\cdot(\vec{p}_f-\vec{p}_i)}. \tag{48}$$

We use the first terms of Eqs. (47) and (48) to estimate the second term of Eq. (44). We immediately expect that this second term is completely negligible because it has the form of the Fourier transform of

$$\frac{1}{\vec{k}'\cdot\vec{k}'+P^2},$$

where $P^2=(\vec{p}_f-\vec{p}_i)^2+2\vec{\kappa}\cdot(\vec{p}_f-\vec{p}_i)$. This Fourier transform falls off very rapidly with $r$, i.e., as $\exp(-Pr)/r$. For typical values of $P$ of about 100 keV$\approx$50 Å$^{-1}$, we will have $Pr\approx25$, where a is the separation ($\sim$2.56 Å). The exponential damping factor destroys this second term. This intuitive conclusion is also confirmed by numerical evaluation, but the strong exponential damping inherent in this term caused the effects of this correction to be too small to be plotted.

### C. Electron propagation

The full expression for the Feynman graphs in Fig. 2 allows a new type of term, one in which the electron propagates over the distance $r$. The mathematical origins of this effect are in the poles of the electron propagator shown in Eq. (25) which arise via the appearance of the four-momentum of the virtual $k'^2\neq0$ in those denominators. There are two terms in that equation, one arising from the uncrossed graph [Fig. 2(a)] and the other from the crossed graph [Fig. 2(b)]. We shall study these terms in sequence, using our standard technique of writing $\vec{k}'=\vec{\kappa}+(\vec{k}'-\vec{\kappa})$ and treating the second term as an expansion parameter—whenever possible without destroying the correct analytic structure.

#### *1. Uncrossed term*

Suppose we keep the full uncrossed term. This means that we must evaluate the integral $J_1(\vec{k},\vec{r})$:

$$J_1(\vec{k},\vec{r})\equiv\int\frac{d^3k'}{(2\pi)^3}\frac{e^{-i(\vec{k}-\vec{k}')\cdot\vec{r}}}{2p_f\cdot k'+k'^2+i\epsilon}\frac{1}{k'^2+i\epsilon}\frac{F(|\vec{k}-\vec{k}'|)}{\omega^2-\vec{k}'^2+i\epsilon}. \tag{49}$$

The product of propagators can be written

$$\frac{1}{2p_f\cdot k'+k'^2}\cdot\frac{1}{k'^2+i\epsilon}=\left[\frac{1}{k'^2+i\epsilon}-\frac{1}{2p_f\cdot k'+k'^2}\right]\frac{1}{2p_f\cdot k'}. \tag{50}$$

The $1/(k'^2+i\epsilon)$ is the photon propagator and we denote its contribution as the photon propagation term; similarly, the second part is the electron propagation term. The last factor $1/(2p_f\cdot k')$ vanishes only when the term in the bracket vanishes and so causes no mathematical difficulty. We may then study two separate integrals

$$J_1(\vec{k},\vec{r})=K_1(\vec{k},\vec{r})+K_2(\vec{k},\vec{r}), \tag{51}$$

where

$$K_1(\vec{k},\vec{r})\equiv\int\frac{d^3k'}{(2\pi)^3}\frac{e^{-i(\vec{k}-\vec{k}')\cdot\vec{r}}}{2p_f\cdot k'}\frac{1}{k'^2+i\epsilon}\frac{F(|\vec{k}-\vec{k}'|)}{\omega^2-\vec{k}'^2+i\epsilon} \tag{52}$$

and

$$K_2(\vec{k},\vec{r})\equiv-\int\frac{d^3k'}{(2\pi)^3}\frac{e^{-i(\vec{k}-\vec{k}')\cdot\vec{r}}}{2p_f\cdot k'+k'^2+i\epsilon}\times\frac{1}{2p_f\cdot k'}\frac{F(|\vec{k}-\vec{k}'|)}{\omega^2-\vec{k}'^2+i\epsilon}. \tag{53}$$

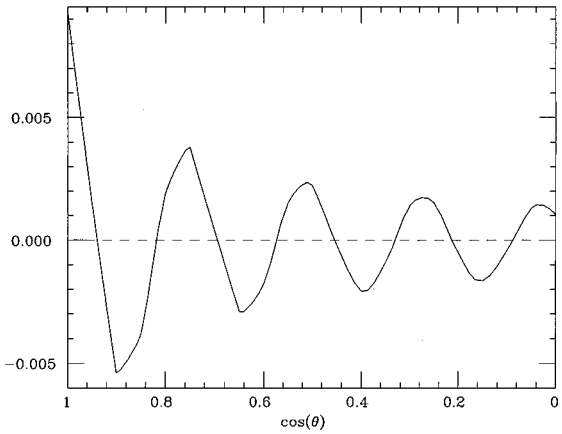


FIG. 8. The small effects of virtual electron propagation in the uncrossed graph in Fig. 2. The real part of the uncrossed correction $\delta J_{\rm on}^{\rm uncr}$ (dashed line) given by Eq. (57) is compared with the real part of the on-shell separated atom approximation $J_{\rm on}$ (solid line) given by Eq. (27). Here $\hat{k}\cdot\hat{p}_f=0.5$ and $\hat{p}_i\cdot\hat{r}=0.5$.

We work first with $K_1$. The manipulations are simplified by using

$$\frac{1}{2p_f\cdot k'}=\frac{1}{2p_f\cdot\kappa}+\frac{1}{2p_f\cdot\kappa}2p_f\cdot(\kappa-k')\frac{1}{2p_f\cdot k'}, \quad (54)$$

where the four-vector $\kappa\equiv(\omega,\vec{\kappa})$. Using this relation in Eq. (52) enables us to derive a differential equation for $K_1$:

$$K_1(\vec{k},\vec{r})=\frac{J_{\rm on}(\vec{k},\vec{r})}{2p_f\cdot\kappa}-\frac{1}{2p_f\cdot\kappa}2\vec{p}_f\cdot\left[\vec{\kappa}-\frac{\vec{\nabla}}{i}-\vec{k}\right]K_1(\vec{k},\vec{r}). \quad (55)$$

We see that the first term is the separated atom approximation for this particular term. The quantity $[\vec{\kappa}+i\vec{\nabla}_r-\vec{k}]$ vanishes when acting on $e^{-i\vec{k}\cdot\vec{r}}e^{i\omega r}/r$, so that the second term is a correction. The effect of this term can be estimated by replacing $K_1$ on the right-hand side by $J_{\rm on}/(2p_f\cdot\kappa)$. Thus

$$(2p_f\cdot\kappa)K_1(\vec{k},\vec{r})\approx J_{\rm on}(\vec{k},\vec{r})+\delta J_{\rm on}^{\rm uncr}(\vec{k},\vec{r}) \quad (56)$$

with

$$\delta J_{\rm on}^{\rm uncr}(\vec{k},\vec{r})\equiv-2\vec{p}_f\cdot[\vec{\kappa}+i\vec{\nabla}_r-\vec{k}]J_{\rm on}(\vec{k},\vec{r}). \quad (57)$$

A brief calculation shows that once again the correction is proportional to the vector integral $\vec{V}_{\rm on}(\vec{k},\vec{r})$ of Eq. (37), and is down by about $1/\omega r$ compared to the first term. Explicit numerical evaluation confirms this estimate, the correction term $J_{\rm on}^{\rm uncr}$ is indeed negligible, as shown in Fig. 8. For general purposes, it is useful to note that Eq. (55) has the formal solution

$$K_1(\vec{k},\vec{r})=\frac{1}{2p_f\cdot\kappa+2\vec{p}_f\cdot(\vec{\kappa}-\vec{k}+i\vec{\nabla}_r)}J_{\rm on}(\vec{k},\vec{r}). \quad (58)$$

This formal solution gives us a controlled way to study some of the corrections to the separated atom approximation.

The $K_2$ term given by Eq. (53) represents new physics occurring in this two-atom process. To see this, recall that $2p_f\cdot k'+k'^2+i\epsilon=(p_f+k')^2-M^2+i\epsilon=(E_f+\omega)^2-m^2-(\vec{p}_f+\vec{k}')\cdot(\vec{p}_f+\vec{k}')+i\epsilon$. We write this in terms of a four-vector $W=(E_f+\omega,\vec{p}_f+\vec{k}')$ as $2p_f\cdot k'+k'^2+i\epsilon=W^2-m^2+i\epsilon$. The zero in this term is a pole in the integrand representing the long distance propagation of the electron of four-momentum $W_{\rm on}=(E_f+\omega,|\vec{p}_f+\vec{k}|\hat{r})$. We use the same pole dominance idea that we used for the photon propagation terms. In this case, the four-vector $W$ appears instead of the four-vector $\kappa$. Then we handle the term $2p_f\cdot k'=2p_f\cdot W-2m^2$ by using

$$\frac{1}{p_f\cdot W-m^2}=\frac{1}{p_f\cdot W_{\rm on}-m^2}+\frac{1}{p_f\cdot W_{\rm on}-m^2}\times p_f\cdot(W_{\rm on}-W)\frac{1}{p_f\cdot W-m^2}. \quad (59)$$

This allows us to derive the analogous differential equation for $K_2$:

$$K_2(\vec{k},\vec{r})=\frac{K_{\rm on}(\vec{k},\vec{r})}{2p_f\cdot W_{\rm on}-m^2}-\frac{1}{2p_f\cdot W_{\rm on}-m^2}\times2\vec{p}_f\cdot\left[\vec{W}_{\rm on}-\left(\frac{\vec{\nabla}}{i}+\vec{k}+\vec{p}_f\right)\right]K_2(\vec{k},\vec{r}), \quad (60)$$

where

$$K_{\rm on}(\vec{k},\vec{r})\equiv-\int\frac{d^3k'}{(2\pi)^3}e^{-i(\vec{k}-\vec{k}')\cdot r}\frac{1}{2p_f\cdot k'+k'^2}\times\frac{F(|\vec{k}-\vec{k}'|)}{\omega^2-\vec{k}'^2+i\epsilon}. \quad (61)$$

Equation (60) is equivalent to the full expression for $K_2$ and also shows how we can make a first approximation for $K_2$ by substituting $K_{\rm on}(\vec{k},\vec{r})/(2p_f\cdot W_{\rm on}-m^2)$ for $K_2$ on the right-hand side. The technique is the same as in previous sections. We immediately see that the second term vanishes in the separated atom approximation.

We may evaluate $K_{\rm on}$ in the separated atom approximation, because this is essentially the same integral as $J_{\rm on}$. The separated atom approximation worked except when $q_1$ was small. Here the quantity $|\vec{k}-|\vec{P}_f+\vec{k}|\hat{r}|$ plays the same role as $q_1$. The result is

$$K_{\rm on}(\vec{k},\vec{r})=e^{-i\vec{k}\cdot\vec{r}}e^{-i\vec{p}_f\cdot\vec{r}}\left(-\frac{1}{4\pi r}\right)\times e^{i\sqrt{2E_f\omega+\omega^2+p_f^2}r}F(|\vec{k}+\vec{p}_f-\sqrt{E_f\omega+\omega^2+p_f^2}\hat{r}|). \quad (62)$$

Since $E_f=\sqrt{m^2+p_f^2}$ is very large, $F$ is evaluated with a large argument, and this kills the $K_2$ term.

The size of the quantity $K_2$ is controlled by $K_{\rm on}$ and by the denominator

$$D\equiv2p_f\cdot W_{\rm on}-m^2=E_f(E_f+\omega)-(\vec{p}_f\cdot\hat{r})|\vec{p}_f+\vec{k}|. \quad (63)$$

Numerical evaluation shows that $K_2\ll K_1$. If $\vec{p}_f=0$, $K_{\rm on}$ is small because the atomic form factor is evaluated at a large

argument. When $|\vec{p}_f|$ takes on a typical experimental value, the energy denominator is very large. The net result is that $K_2$ is ignorable.

However when $|\vec{p}_f|$ is very much larger than the electron mass, $D$ approaches 0 and $K_2$ can become large. The bremsstrahlung from a collection of atoms would then have a large contribution from the electron propagation term. This small value of $D$ is a necessary condition for the occurrence of the Landau-Pomeranchuk-Migdal (LPM) effect[31] in which the long time scale of electron propagation allows a coherent effect which reduces the radiation. However, we are concerned with the low energy limit in which the electron momentum is much less than its mass. So, for us, the electron propagation term is negligible.

### 2. Crossed term

Suppose we keep the full crossed term. This means that we must evaluate the integral $J_2(\vec{k},\vec{r})$:

$$J_2(\vec{k},\vec{r})\equiv\int\frac{d^3k'}{(2\pi)^3}\frac{e^{-i(\vec{k}-\vec{k}')\cdot\vec{r}}}{2p_i\cdot k'-k'^2+i\epsilon}\frac{1}{k'^2+i\epsilon}\frac{F(|\vec{k}-\vec{k}'|)}{\omega^2-\vec{k}'^2+i\epsilon}. \tag{64}$$

The product of propagators can be written

$$\frac{1}{2p_i\cdot k'-k'^2}\cdot\frac{1}{k'^2+i\epsilon}=\left[\frac{1}{k'^2+i\epsilon}+\frac{1}{2p_i\cdot k'-k'^2}\right]\frac{1}{2p_i\cdot k'}. \tag{65}$$

Again we denote the first term as the photon propagation term and the second term as the electron propagation term. The last factor $1/(2p_i\cdot k')$ vanishes only when the term in the bracket vanishes, so this zero residue pole makes no contribution to the integral $J_2(\vec{k},\vec{r})$. We may then study two separate integrals

$$J_2(\vec{k},\vec{r})=K_3(\vec{k},\vec{r})+K_4(\vec{k},\vec{r}), \tag{66}$$

where

$$K_3(\vec{k},\vec{r})\equiv\int\frac{d^3k'}{(2\pi)^3}\frac{e^{-i(\vec{k}-\vec{k}')\cdot\vec{r}}}{2p_i\cdot k'}\frac{1}{k'^2+i\epsilon}\frac{F(|\vec{k}-\vec{k}'|)}{\omega^2-\vec{k}'^2+i\epsilon} \tag{67}$$

and

$$K_4(\vec{k},\vec{r})\equiv\int\frac{d^3k'}{(2\pi)^3}\frac{e^{-i(\vec{k}-\vec{k}')\cdot\vec{r}}}{2p_i\cdot k'-k'^2+i\epsilon}\frac{1}{2p_i\cdot k'}\frac{F(|\vec{k}-\vec{k}'|)}{\omega^2-\vec{k}'^2+i\epsilon}. \tag{68}$$

It is clear that we can handle $K_3$ using the same techniques that we used for $K_1$. We derive the following differential equation for $K_3$:

$$K_3(\vec{k},\vec{r})=\frac{J_{\rm on}(\vec{k},\vec{r})}{2p_i\cdot\kappa}-\frac{1}{2p_i\cdot\kappa}2\vec{p}_i\cdot\left[\vec{\kappa}-\frac{\vec{\nabla}_r}{i}-\vec{k}\right]K_3(\vec{k},\vec{r}). \tag{69}$$

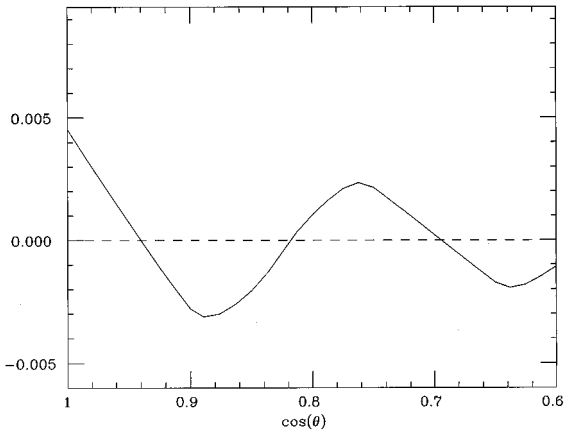


FIG. 9. The small effects of virtual electron propagation in the crossed graph in Fig. 2. The real part of the crossed correction $\delta J_{\rm on}^{\rm cr}$ (dashed line) given by Eq. (72) is compared with the real part of the on-shell separated atom approximation $J_{\rm on}$ (solid line) given by Eq. (27). Here $\hat{p}_i\cdot\hat{r}=0.5$.

Once again the first term is the separated atom approximation for this particular term. This dominates $K_3$. For general purposes, it is useful to note that Eq. (69) has the formal solution

$$K_3(\vec{k},\vec{r})=\frac{1}{2p_i\cdot\kappa+2\vec{p}_i\cdot(\vec{\kappa}-\vec{k}+i\vec{\nabla}_r)}J_{\rm on}(\vec{k},\vec{r}). \tag{70}$$

Again, this formal solution gives us a controlled way to study the corrections to the separated atom approximation. We use

$$(2p_i\cdot\kappa)K_3(\vec{k},\vec{r})=J_{\rm on}(\vec{k},\vec{r})+\delta J_{\rm on}^{\rm cr}(\vec{k},\vec{r}) \tag{71}$$

with

$$\delta J_{\rm on}^{\rm cr}(\vec{k},\vec{r})\equiv-2\vec{p}_i\cdot[\vec{\kappa}+i\vec{\nabla}_r-\vec{k}]J_{\rm on}(\vec{k},\vec{r}). \tag{72}$$

We find the crossterm correction effects due to $\delta J_{\rm on}^{\rm cr}$ are very small, as illustrated in Fig. 9.

The term $K_4$ of Eq. (68) represents new physics occurring in this two-atom process. We use the same techniques we used for $K_2$. There is a pole in the integrand representing the long distance propagation of the electron of four-momentum $X_{\rm on}=(E_i-\omega,|\vec{p}_i-\vec{k}|\hat{r})$. This allows us to derive the differential equation

$$K_4(\vec{k},\vec{r})=\frac{L_{\rm on}(\vec{k},\vec{r})}{2p_i\cdot X_{\rm on}+m^2}-\frac{1}{2p_i\cdot X_{\rm on}-m^2}\times2\vec{p}_i\cdot\left[\vec{X}_{\rm on}-\left(\frac{\vec{\nabla}_r}{i}+\vec{k}+\vec{p}_i\right)\right]K_4(\vec{k},\vec{r}), \tag{73}$$

where

$$L_{\rm on}(\vec{k},\vec{r})\equiv-\int\frac{d^3k'}{(2\pi)^3}e^{-i(\vec{k}-\vec{k}')\cdot r}\frac{1}{2p_i\cdot k'-k'^2}\times\frac{F(|\vec{k}-\vec{k}'|)}{\omega^2-\vec{k}'^2+i\epsilon}. \tag{74}$$

Note the appearance of the $+m^2$ term in the denominator of the first term of $K_4$. This renders the energy denominator very large, it never vanishes even for infinitely large $E_i$. Careful numerical evaluation leads to negligibly small results for $K_4$. These results are too small to be plotted.

### D. Summary of bremsstrahlung cross section with Thompson scattering

The basic expression for the bremsstrahlung holography cross section where the object atom scattering can be described by the Thompson amplitude is given by Eqs. (21) and (22). The full on- and off-shell integral $I(\vec{k},\vec{r})$ of Eq. (23) is very well approximated by the on-shell integral $I_{\rm on}(\vec{k},\vec{r})$ of Eq. (26).

Furthermore, $\kappa_\mu\kappa^\mu=0$ so that we may perform the sum over the polarization vectors $\hat{\epsilon}$ [see Ref. 25, Eq. (7.61)] with the results

$$\sum_\epsilon \hat{\epsilon}\cdot\vec{V}(k)\hat{\epsilon}\cdot\vec{V}(k)=\frac{2p_f\cdot p_i}{p_f\cdot kp_i\cdot k}-\frac{m^2}{(p_f\cdot k)^2}-\frac{m^2}{(p_i\cdot k)^2} \tag{75}$$

and

$$\sum_\epsilon \hat{\epsilon}\cdot\vec{V}(k)\hat{\epsilon}\cdot\vec{V}(\kappa)=\frac{p_f\cdot p_i}{p_f\cdot kp_i\cdot\kappa}+\frac{p_f\cdot p_i}{p_f\cdot\kappa p_i\cdot k}-\frac{m^2}{p_f\cdot kp_f\cdot\kappa}-\frac{m^2}{p_i\cdot kp_i\cdot\kappa}. \tag{76}$$

The net result is that

$$\sum_\epsilon \overline{|\mathcal{M}|^2}=\left(\frac{Ze^3}{|\vec{q}|^2}[1-F(|\vec{p}_f-\vec{p}_i+\vec{k}|)]\right)^2\left[\frac{2p_f\cdot p_i}{p_f\cdot kp_i\cdot k}-\frac{m^2}{(p_f\cdot k)^2}-\frac{m^2}{(p_i\cdot k)^2}\right]$$
$$+\frac{Z^3e^8}{|\vec{q}|^2}[1-F(|\vec{q}|)]\frac{[1-F(|\vec{p}_f-\vec{p}_i+\vec{\kappa}|)]}{|\vec{p}_f-\vec{p}_i+\vec{\kappa}|^2}\frac{2}{m}\mathrm{Re}J_{\rm on}(\vec{k},\vec{r})\left[\frac{p_f\cdot p_i}{p_f\cdot kp_i\cdot\kappa}+\frac{p_f\cdot p_i}{p_f\cdot\kappa p_i\cdot k}-\frac{m^2}{p_f\cdot kp_f\cdot\kappa}-\frac{m^2}{p_i\cdot kp_i\cdot\kappa}\right]. \tag{77}$$

The factors in the square brackets account for the peaking of the bremsstrahlung radiation intensity which occurs in the direction of the initial electron velocity. This feature represents the influence of the vector nature of the photon and is significantly different than the simple classical result from scalar electrodynamics.

The polarization dependent cross section is obtained simply from Eq. (22). by replacing the term $I(\vec{k},\vec{r})$ with $I_{\rm on}$ of Eq. (26). That is, we find

$$\overline{|\mathcal{M}(\epsilon)|^2}\equiv\left(\frac{Ze^3}{|\vec{q}|^2}[1-F(|\vec{p}_f-\vec{p}_i+\vec{k}|)]\right)^2[\hat{\epsilon}\cdot\vec{V}(k)\hat{\epsilon}\cdot\vec{V}(k)]\frac{Z^3e^8}{|\vec{q}|^2}\frac{2[1-F(|\vec{q}|)]}{m}\mathrm{Re}I_{\rm on}(\vec{k},\vec{r}). \tag{78}$$

## VI. BREMSSTRAHLUNG X-RAY HOLOGRAPHY (BXH) INCLUDING RESONANT SCATTERING

We now return to the case where the scattering of the bremsstrahlung photon by the object atoms includes the resonance correction terms given by Eqs. (15), (17), and (18). We simply use those equations in the expression for the amplitude given by Eq. (10). The total Thompson plus resonant hologram amplitude $\mathcal{M}_{T+R}$ is the sum of the Born approximation reference term $\mathcal{R}$ and the Thompson plus resonant object amplitude $\mathcal{O}$. Calculating this amplitude and squaring leads to the resonance correction $\overline{|\delta\mathcal{M}_R|^2}$ to the nonresonant Thompson squared matrix element $\overline{|\mathcal{M}|^2}$ with

$$\overline{|\delta\mathcal{M}_R|^2}\equiv+\frac{Z^2e^6[1-F(|\vec{q}|)]}{|\vec{q}|^2}S(\omega)2\mathrm{Re}\hat{\epsilon}\cdot\vec{V}(k)\int\frac{d^3k'}{(2\pi)^3}\hat{\epsilon}\cdot\vec{V}_1(k')e^{-i(\vec{k}-\vec{k}')\cdot\vec{r}}\left(\frac{[1-F(|\vec{q}'|)]}{|\vec{q}'|^2}\frac{F(|\vec{k}-\vec{k}'|)}{\omega^2-\vec{k}'^2+i\epsilon}\right), \tag{79}$$

where $S(\omega)$ is given by Eq. (18). If the resonant scattering and the Thompson scattering terms are of comparable strength, the full square of the resonant and nonresonant hologram amplitude is the sum of the terms given by Eqs. (77) and (79):

$$\overline{|\mathcal{M}_{T+R}|^2}=\overline{|\mathcal{M}|^2}+\overline{|\delta\mathcal{M}_R|^2}. \tag{80}$$

The integral over $d^3k'$ is the same as that evaluated in the previous sections. The essential result is that the integral can be evaluated by removing the expression $\vec{V}_1(k')[1-F(|\vec{q}'|)]/|\vec{q}'|^2$ and evaluating it for $k'=\kappa$. Recall that $\kappa=(\omega,\omega\hat{r})$. In that case,

$$\overline{|\delta\mathcal{M}_R|^2}=+\frac{Z^2e^6[1-F(|\vec{q}|)]}{|\vec{q}|^2}S(\omega)2\mathrm{Re}J_{\rm on}(\vec{k},\vec{r})\hat{\epsilon}\cdot\vec{V}(k)\hat{\epsilon}\cdot\vec{V}(\kappa)\frac{[1-F(|\vec{p}_f-\vec{p}_i+\vec{\kappa}|)]}{|\vec{p}_f-\vec{p}_i+\vec{\kappa}|^2}. \tag{81}$$

As explained above, the diagrams with propagating electrons are also potentially troublesome—at high energies these effects produce the interesting LPM effects. Here the off-shell electron effects are governed by known atomic wave functions which go into computing the function $S(\omega)$.

The sum over the polarization vectors of the photon leads to the expression

$$\sum_{\epsilon} \overline{|\delta\mathcal{M}_R|^2} = + \frac{Z^2 e^6 [1-F(|\vec{q}|)]}{|\vec{q}|^2} S(\omega) 2\mathrm{Re} J_{\mathrm{on}}(\vec{k},\vec{r}) \frac{[1-F(|\vec{p}_f-\vec{p}_i+\vec{\kappa}|)]}{|\vec{p}_f-\vec{p}_i+\vec{\kappa}|^2} \left[ \frac{p_f\cdot p_i}{p_f\cdot k p_i\cdot \kappa} + \frac{p_f\cdot p_i}{p_f\cdot \kappa p_i\cdot k} - \frac{m^2}{p_f\cdot k p_f\cdot \kappa} - \frac{m^2}{p_i\cdot k p_i\cdot \kappa} \right]. \tag{82}$$

## VII. X-RAY FLUORESCENCE HOLOGRAPHY (XFH)

We now briefly consider the physics of x-ray fluorescence holography (XFH). In this case, an atom in the sample is excited from its ground state into an excited state by an incoming photon or an incoming electron. After the ionization, the excited atom decays and we must consider the interference effects for the outgoing fluorescence photon via the direct path to the detector and via the single-scattering paths to the detector.

The Feynman diagrams for XFH are shown in Fig. 10. Suppose the incident photon [Fig. 10(a)]—or the incident electron [Fig. 10(b)]—interacts with an atom, knocking an $s$-shell electron into a continuum wave function $c$. A $p$-shell electron can spontaneously decay to the $s$ state, emitting a fluorescence photon with the characteristic energies of the atom $\omega = E_p - E_s$, and with the reference amplitude $\mathcal{R}_{\mathrm{psf}(c\to i)}(\vec{k},\hat{\epsilon})$ for photostimulated fluorescence, or with the reference amplitude $\mathcal{R}_{\mathrm{esf}(c\to i)}(\vec{k},\hat{\epsilon})$ for electron stimulated fluorescence.

First, consider the ionization process. For photoionization, the incoming photon is real or on shell. For electron induced ionization, the incoming electron is on shell and the ionization occurs via the virtual photon exchange, but the potential off-shell photon effects are exactly the same as the bremsstrahlung case we have already analyzed in detail. For the relatively low energies used in the current XFH experiments, these effects are completely negligible.

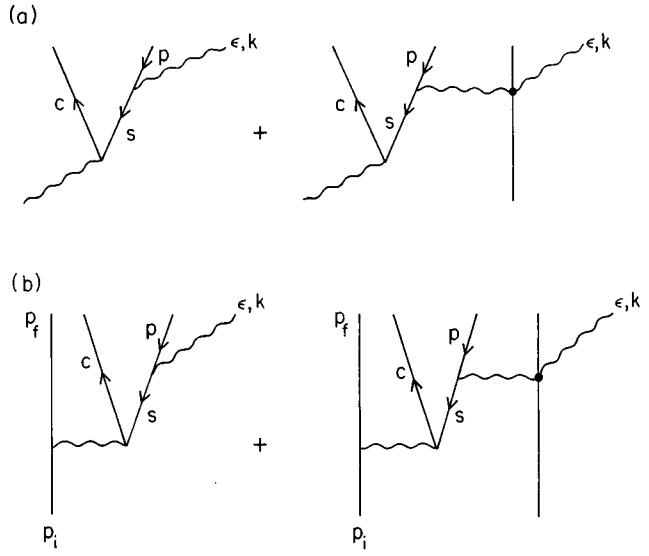


FIG. 10. The Feynman diagrams for x-ray fluorescence holography (XFH). The $s$-state core hole can be made by photoionization (a), or by electron induced ionization (b). The black dot represents the photon-object atom scattering amplitude, $c$ the continuum electron, $p$ the $p$-state electron, and $s$ the $s$-state electron. Note that the black dot is shorthand for two diagrams—namely, the crossed and uncrossed Compton diagrams shown in Fig. 3.

Second, consider the intermediate states. What are the possible off-shell electron effects? The electron promoted into the continuum is detectable and is therefore on shell. The virtuality of the continuum electron enters only if there is another final state interaction; such effects are of higher order in $\alpha$ and are neglected here. Thus the only possible off-shell electron effects come from the virtual intermediate state electron in the $s$ state. But this is governed by well-known atomic wave functions.

For the characteristic radiation used in XFH, the long wavelength approximation holds and the radiation is dominated by the electric dipole process. This predominantly dipole character, combined with the fact that the initial and final electron is on shell, indicates immediately that the separated atom approximation will be extremely close to the exact quantum electrodynamic solution. Thus the holographic reference amplitude takes the simple form

$$\mathcal{R}_{\mathrm{psf}(c\to i)}(\vec{k},\hat{\epsilon}) = \omega T_{\mathrm{psf}}(\vec{k},\hat{\epsilon}) \tag{83}$$

for photoionization, and

$$\mathcal{R}_{\mathrm{esf}(c\to i)}(\vec{k},\hat{\epsilon}) = \omega T_{\mathrm{esf}}(\vec{k},\hat{\epsilon}) \tag{84}$$

for electron ionization, where the $T_{\mathrm{psf}}(\vec{k},\hat{\epsilon})$ and $T_{\mathrm{esf}}(\vec{k},\hat{\epsilon})$ factors account for the remainder of the atomic matrix element.

The holographic object amplitude contribution to the total amplitude occurs because the photon is scattered coherently by the object atoms. When the Thompson rescattering effects dominate, the on-shell approximations for the FXH holographic interference terms are given by the expressions

$$\mathcal{M}^{\mathrm{on}}_{\mathrm{psf}}(\vec{k},\hat{\epsilon}) = \omega T_{\mathrm{psf}}(\vec{k},\hat{\epsilon}) \left( 1 - \frac{e}{m} J_{\mathrm{on}}(\vec{k},\vec{r}) \right) \tag{85}$$

for photon stimulated XFH, and

$$\mathcal{M}^{\mathrm{on}}_{\mathrm{esf}}(\vec{k},\hat{\epsilon}) = \omega T_{\mathrm{esf}}(\vec{k},\hat{\epsilon}) \left( 1 - \frac{e}{m} J_{\mathrm{on}}(\vec{k},\vec{r}) \right) \tag{86}$$

for electron stimulated XFH. Here the integral $J_{\mathrm{on}}(\vec{k},\vec{r})$ is given by Eqs. (27) and (32).

The cross section is obtained by squaring the amplitude and summing over the polarization vectors of the photon.

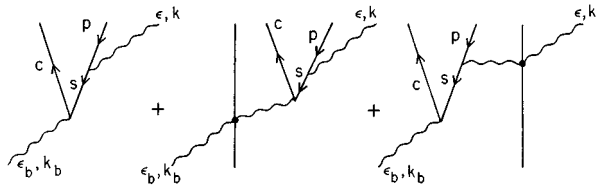


FIG. 11. The Feynman diagrams for multiple energy x-ray holography (MEXH). The notation is the same as Fig. 10.

Thus the cross section for the intensity of the XFH hologram in the on-shell approximation is given generically by

$$\frac{d\sigma}{d\Omega}=\omega^2|T(\vec{k},\hat{\epsilon})|^2\left(1-2\frac{e}{m}\mathrm{Re}J_{\mathrm{on}}(\vec{k},\vec{r})\right). \quad (87)$$

And again, when the high electron density regions of the atoms are sufficiently well separated, we will recover the usual classical holographic form in the far field limit via Eq. (30).

## VIII. MULTIPLE-ENERGY X-RAY HOLOGRAPHY (MEXH)

Finally, we consider very briefly the physics of multiple-energy x-ray holography (MEXH). In this case, a real photon is sent into the sample from outside and we must consider the interference between the direct path to the detector atom and the single-scattering paths via the object atoms to the detector atom. The Feynman diagrams for this interference are shown in Fig. 11. Note that the Feynman diagrams for MEXH are not just the time reversed Feynman diagrams for photon induced XFH, and that there are three interfering terms in MEXH.

Within classical electrodynamics, MEXH has been related to XFH by the reciprocity theorem, which can be paraphrased roughly as follows: Put the source outside the sample and the detector inside the sample, turn on the source, and measure the electric field at the detector; if the positions of the source and the detector are interchanged, the electric field measured at the detector will be the same. This result comes from the time reversal invariance of Maxwell's equations.

How does this very reasonable classical result emerge from the quantum electrodynamic treatment? It clearly is not just simple time reversal invariance, since there are three interfering diagrams in MEXH and only two interfering diagrams in XFH. There are three diagrams in MEXH because the incoming photons interfere to produce the atomic excitations that lead to the fluorescence, and the outgoing fluorescence photons interfere just as they do in XFH. However since MEXH must average over many outgoing directions to increase the signal level, the interference effects in the outgoing photons will be washed out,[32] and we need only consider the first two diagrams in Fig. 11. Then our question becomes how are these two diagrams related to the analogous diagrams for XFH shown in Fig. 10. They still are not just the simple time reversed diagrams: in MEXH the Thompson process (or, in general, the Compton process) occurs in the incoming state of the photon that will produce the photoionization, whereas in XFH the Thompson process is in the outgoing photon state of energy $(E_p-E_s)$ that will be detected. Since the incoming photon energy used in MEXH is not equal to $(E_p-E_s)$, the two processes are not related by time reversal invariance.

We discuss this further by displaying the relevant equation. In MEXH, the holographic object amplitude contribution to the total amplitude occurs because the initial photon in the incoming beam with momentum $k_b$ and polarization $\hat{\epsilon}_b$ is scattered elastically by the object atoms prior to absorption by the detector atom. If the total matrix element to produce the outgoing angle averaged MEXH fluorescence decay is denoted $\mathcal{R}_{\mathrm{me}(c\to i)}(\vec{k}_b,\hat{\epsilon}_b)$ and if the Thompson scattering effects dominate, then the on-shell approximation for the holographic interference term is given by the expression

$$\mathcal{M}^{\mathrm{on}}_{\mathrm{me}}(\vec{k}_b,\hat{\epsilon}_b)=\left(1-\frac{e}{m}J_{\mathrm{on}}(\vec{k}_b,\vec{r})\right)\omega T_{\mathrm{me}}(\vec{k}_b,\hat{\epsilon}_b), \quad (88)$$

where $\omega T_{\mathrm{me}}(\vec{k}_b,\hat{\epsilon}_b)$ represents the photon absorption process, and once again the integral $J_{\mathrm{on}}(\vec{k}_b,\vec{r})$ is given by Eqs. (27) and (32). The amplitude for MEXH given by Eq. (88) and the amplitude for FXH given by Eqs. (85) and (86) are not complex conjugates of one another. However, the physics of these two amplitudes is closely related.

## IX. SUMMARY AND DISCUSSION

We have shown that, if the energy of the bremsstrahlung photons is measured, the bremsstrahlung radiation produced inside a crystal will produce a holographic interference pattern in the far field outside the crystal. To use this new form of generalized holography,[33] we must know the reference and object amplitudes. These amplitudes were calculated using quantum electrodynamics, and compared with the corresponding predictions of classical scalar electrodynamics. The essential results for bremsstrahlung holography are displayed in Eqs. (77), (78), and (82).

The total amplitude $\mathcal{M}$ is the sum of the reference amplitude $\mathcal{R}$ and the object amplitude $\mathcal{O}$. To obtain very accurate results, the full expression for the quantity $J_{\mathrm{on}}(\vec{k},\vec{r})$ given by Eq. (32) must be used. Its simpler asymptotic form given by Eq. (30) is not accurate for the case in which the separation $\vec{r}$ between the source atom and the object atom is parallel to the direction $\hat{k}$ of the detected photon, as shown in Fig. 5.

The key feature in obtaining Eqs. (77) and (82) is that the photons that propagate from the source atom to the object atoms are essentially on-shell—the square of their four-momenta is very close to zero. Section V is devoted to the detailed arguments for our on-shell separated atom approximation. We show explicitly that all of the known short ranged off-shell virtual effects are negligibly small for the low (40–60 keV) electron energies used in the current experiments. The underlying reason for this is that the atoms in solids are too far apart for the off-shell photons or electrons, produced via bremsstrahlung or via fluorescence, to propagate from one atom to another.

It is interesting to compare the present case in which photons propagate between atoms with two examples from nuclear physics: (1) hadronic scattering from nuclei, and (2) pion production in nucleon-nucleon or nucleon-nucleus collisions. Beg's theorem[34] applies to hadron-nuclear scattering and states that, if the target nucleons are separated by dis-

tances greater than the range of the hadron-nucleon interaction, then the hadron-nucleus scattering amplitude can be expressed in terms of on-shell hadron nucleon scattering amplitudes. This is called the separated scatterer approximation.[17–20] In this language, our results can be stated as the confirmation that the analogous separated atom approximation is valid.

In our first example, we want to consider the scattering of hadrons from the nucleons inside the nucleus. In our condensed matter physics example, we were able to consider the scattering of photons from essentially stationary atoms and slowly moving electrons. However, in nuclei, the nucleons move extremely rapidly so that the separations between the nucleons fluctuate and, in addition, the nucleons can overlap. The average separation distance between nucleons is about 1.8 fm, which is about twice as big as the typical range of hadron-nucleon interactions ($\sim$1 fm). However, in the case of very high energy hadronic beams, we can be reasonably sure that the nucleons will not move during the passage of the hadron through the target, and that the use of on-shell hadron nucleon amplitudes based on the average separation distance is valid

In our second example, the pion ($\pi$) production reactions $pp \rightarrow d\pi$ or $p+A \rightarrow (A+1)\pi^+$, are the strong interaction analogs of bremsstrahlung holography. In this case, Fig. 2 also applies, but the wiggly lines represent pions and the solid vertical lines represent nucleons or nuclei. These processes involve high momentum transfer (for pions produced with low energy) and small internucleon separations. Therefore off-shell pions can and do propagate between nucleons. As a result, no cross sections can be computed to better than about a factor of 2.[35] In contrast, in this present paper, we can calculate cross sections reliably at the $10^{-4}$ level or better because the atoms and the electrons in the atoms move relatively slowly.

The separability argument works extremely well for the three x-ray holographies (FXH, MEXH, and BXH) currently under experimental development. In a sense, it is quantum electrodynamics that requires the separated atom approximation to work so well since it supplies the forces responsible for the relatively slow motion of the atoms and of the electrons in the atoms, and it also supplies the interactions between the atoms and the incoming and outgoing photons and electrons.

Thus it is quantum electrodynamics that gives us our main results for bremsstrahlung holography summarized in Eqs. (21)–(25), Eq. (77), and Eq. (82). Quantum electrodynamics shows that bremsstrahlung holography should work—the remaining problems are experimental.

## ACKNOWLEDGMENTS

We gratefully acknowledge the partial support of this work by the U.S. Department of Energy under Grant Nos. DE-FG03-97ER41014 and DE-FG06-88ER40427, by the Japanese New Energy and Industrial Technology Development Organization, and by the University of Washington Research Royalty Fund under Grant No. 65-9976. One of us (G.A.M.) thanks the National Institute for Nuclear Theory for partial support during the completion of this work. We thank Professor John Rehr for supplying us with the isolated atom and embedded atom electron densities for crystalline copper shown in Fig. 4 and Professor A. Lande for a useful discussion.

[1] D. Gabor, Nature (London) **161**, 777 (1948); Proc. R. Soc. London, Ser. A **197**, 454 (1949); Proc. R. Soc. London, Ser. B **64**, 449 (1951).

[2] D. Gabor, *Nobel Lectures in Physics 1971–1980* (World Scientific, Singapore, 1992), p. 12; Science **177**, 299 (1972).

[3] A. Szöke, in *Short Wavelength Coherent Radiation: Generation and Applications*, edited by D.T. Attwood and J. Boker, AIP Conf. Proc. No. **147 (AIP**, New York, 1986), p. 361.

[4] There are so many papers on electron holography that it is impossible for us to provide all the references. Since our paper is on x-ray holography, we have tried only to provide an entry into the literature based on recent papers. We certainly do not mean to imply that the recent papers we have quoted for this purpose properly give credit for the extensive work in electron holography.

[5] For an entry into the photoelectron holography literature, see, for example, R. Denecke *et al*., Surf. Sci. **331-3**, 1085 (1995); J.M. Roesler *et al*., *ibid*. **329**, L588 (1995); S.Y. Tong, H. Li, and H. Huang, Phys. Rev. B **51**, 1850 (1995); L. Fonda, Phys. Status Solidi B **188**, 599 (1995); L.J. Terminello *et al*., in *Determining Nanoscale Physical Properties of Materials by Microscopy and Spectroscopy*, edited by M. Sarikaya, H.K. Wickramasighe, and M. Isaacson, MRS Symposia Proceedings No. 332 (Materials Research Society, Pittsburgh, 1994), p. 141; D.P. Woodruff and A.M. Bradshaw, Rep. Prog. Phys. **57**, 1029 (1994); M.T. Sieger *et al*., Phys. Rev. Lett. **73**, 3117 (1994); C.M. Wei *et al*., Chem. Phys. Lett. **228**, 513 (1994); C.S. Fadley *et al*., J. Electron Spectrosc. Relat. Phenom. **68**, 19 (1994); J. Osterwalder *et al*., *ibid*. **68**, 1 (1994); M. Zharnikov *et al*., Surf. Sci. **312**, 82 (1994); M. Zharnikov *et al*., *ibid*. **306**, 125 (1994); B.L. Petersen *et al*., Chem. Phys. Lett. **220**, 46 (1994), and references therein.

[6] For an entry into the Auger electron holography literature, see, for example, D.P. Woodruff, Surf. Sci. **299-300**, 183 (1994); D.K. Saldin, G.R. Harp, and B.P. Tonner, Phys. Rev. B **45**, 9629 (1992); P. Hu and D.A. King, Nature (London) **353**, 831 (1991); G.R. Harp, D.K. Saldin, and B.P. Tonner, Phys. Rev. B **42**, 9199 (1990), and references therein.

[7] For an entry into the diffuse LEED holography literature, see, for example, A. Szöke, Phys. Rev. B **47**, 14 044 (1993); P. Hu and D.A. King, Appl.Surf. Sci. **70-71**, 396 (1993); K. Heinz *et al*., *ibid*. **70-71**, 367 (1993); D.K. Saldin *et al*., Phys. Rev. Lett. **70**, 1112 (1993); S.Y. Tong, H. Huang, and X.Q. Guo, *ibid*. **69**, 3654 (1992); P. Hu and D.A. King, Nature (London) **360**, 6405 (1992); C.M. Wei and S.Y. Tong, Surf. Sci. **274**, L577 (1992); D.L. Saldin, G.R. Harp, and B.P. Tonner, Phys. Rev. B **45**, 9629 (1992); M.A. Mendez *et al*., *ibid*. **45**, 9402 (1992); M.A. Mendez, C. Gluck, and K. Heinz, J. Phys. Condens. Matter **4**, 999 (1992); P.L. de Andres, Phys. Scr. **T39**, 318 (1991); P.L. de Andres, Surf. Sci. **269-270**, 1 (1991), and references therein.

[8] For an entry into the diffuse Kikuchi holography literature, see,

for example, H. Zhao *et al*., Surf. Sci. **315**, L1007 (1994); P. Hu and D.A. King, Nature (London) **353**, 831 (1991); G.R. Harp, D.K. Saldin, and B.P. Tonner, Phys. Rev. Lett. **65**, 1012 (1990), and references therein.

[9] M. Tegze and G. Faigel, Europhys. Lett. **16**, 41 (1991).

[10] C.S. Fadley, in *Applications of Synchrotron Radiation Techniques to Materials Science*, edited by D. L. Perry, N. Shinn, R. Stockbauer, K. D'Amico, and L. Terminello, MRS Symposia Proceedings No. 307 (Materials Research Society, Pittsburgh, 1993), p. 261; P.M. Len *et al*., Phys. Rev. B **50**, 11 275 (1994).

[11] M. Tegze and G. Faigel, Nature (London) **380**, 49 (1996).

[12] T. Gog *et al*., Phys. Rev. Lett. **76**, 3132 (1996); Synch. Rad. News **9**, 30 (1996); P.M. Len *et al*. (unpublished).

[13] For an entry into the multiple-energy electron holography literature, see, for example, J.J. Barton and L.J. Terminello, in *Structure of Surfaces III*, edited by S.Y. Tong *et al*. (Springer-Verlag, Berlin, 1991), p. 107; S.Y. Tong, H. Li, and H. Huang, Phys. Rev. Lett. **67**, 3102 (1991); J.J. Barton, *ibid*. **67**, 3106 (1991); S.Y. Tong, H. Huang, and H. Li, in *Advances in Surface and Thin Film Diffraction*, edited by T.C. Huang, P.J. Cohen, and D.J. Eaglesham, MRS Symposia Proceedings No. 208 (Materials Research Society, Pittsburgh, 1991), p. 13; H. Huang, H. Li, and S.Y. Tong, Phys. Rev. B **44**, 3240 (1991); L.J. Terminello, J.J. Barton, and D.A. Lapiano-Smith, J. Vac. Sci. Technol. B **10**, 2088 (1992); Phys. Rev. Lett. **70**, 599 (1993), and references therein.

[14] S.G. Bompadre, T.W. Petersen, and L.B. Sorensen (unpublished).

[15] J.J. Barton, Phys. Rev. Lett. **61**, 1356 (1988).

[16] P.J. Rous and M.H. Rubin, Surf. Sci. Lett. **316**, L1068 (1994).

[17] D. Agassi and A. Gal, Ann. Phys. (N.Y.) **75**, 56 (1973).

[18] L. Foldy and J.D. Walecka, Ann. Phys. (N.Y.) **54**, 449 (1969).

[19] L.S. Rodberg and R.M. Thaler, *Introduction to the Quantum Theory of Scattering* (Academic Press, New York, 1967).

[20] M. Ericson and T.E.O. Ericson, Ann. Phys. (N.Y.) **36**, 383 (1966).

[21] When the crystal is nearly perfect, we must use the dynamic theory of x-ray diffraction instead of the kinematic theory. In the dynamical scattering limit, the incoming particles coherently multiply scatter from many atoms in the crystal. The interference between these many multiple-scattering events produces the Bragg-Darwin peaks.

[22] H. Winick *et al*., Nucl. Instrum. Methods Phys. Res. A **347**, 199 (1994).

[23] J.R. Breedlove, Jr. and G.T. Trammel, Science **170**, 1310 (1970); I. McNulty, Nucl. Instrum. Methods Phys. Res. A **347**, 170 (1994).

[24] J.P. Hannon and G.T. Trammel, *Mossbauer Effect Methodology* (Plenum, New York, 1974), Vol. 9, p. 181; J.P. Hannon, N.J. Carron, and G.T. Trammel, Phys. Rev. B **9**, 2791 (1974); J.T. Hutton, G.T. Trammel, and J.P. Hannon, *ibid*. **31**, 743 (1985); **31**, 6420 (1985).

[25] J.D. Bjorken and S.D. Drell, *Relativistic Quantum Mechanics* (McGraw-Hill, New York, 1964).

[26] G. Elwert and E. Hauge, Phys. Rev. **183**, 90 (1969); G. Elwert, *Physics of One- and Two-Electron Atoms* (North-Holland, Amsterdam, 1969); G. Elwert, Ann. Phys. (Leipzig) **34**, 178 (1939).

[27] R.H. Pratt *et al*., At. Data Nucl. Data Tables **20**, 175 (1977); **26**, 477 (1981); S.M. Seltzer and M.J. Berger, *ibid*. **35**, 345 (1986).

[28] J.J. Sakurai, *Advanced Quantum Mechanics* (Addison-Wesley, Reading, MA, 1967).

[29] J.D. Jackson, *Classical Electrodynamics* (Wiley, New York, 1975).

[30] S.I. Zabinsky *et al*., Phys. Rev. B **52**, 2995 (1996); J.J. Rehr (private communication).

[31] L.D. Landau and I.J. Pomeranchuk, Dokl. Akad. Nauk. SSSR **92**, 535 (1953); **92**, 735 (1953); A.B. Migdal, Phys. Rev. **103**, 1811 (1956); S.R. Klein *et al*., in *Lepton and Photon Interactions*, edited by Persis Drell and David Rubin, AIP Conf. Proc. No. **302** (AIP, New York, 1994), p. 172.

[32] However, even the complete $4\pi$ outgoing angle averaged MEXH will still contain a subtle modulation which is the photon equivalent of XAFS, but these photon-XAFS-like oscillations in the angle averaged MEXH fluorescence will be very small and can be neglected in experimental MEXH. This photon XAFS provides only spherically averaged distances like electron XAFS.

[33] R.P. Porter, *Progress in Optics* (North-Holland, Amsterdam, 1989), Vol. XXVII, p. 317.

[34] M.A. Bèg, Ann. Phys. (N.Y.) **13**, 110 (1961).

[35] D.F. Measday and G.A. Miller, *Annual Reviews of Nuclear Science* (Annual Reviews, Palo Alto, 1979), Vol. 29, p. 121; H.W. Fearing, Prog. Part. Nucl. Phys. **7**, 113 (1981).

# Tabletop Bremsstrahlung X-Ray Holography: Making Multiwavelength X-Ray Holograms

S. G. Bompadre,* T. W. Petersen, and L. B. Sorensen
*Department of Physics, University of Washington, Seattle, Washington 98195-1560*
(Received 2 December 1998)

We have used a tabletop x-ray holography apparatus to measure the bremsstrahlung x-ray intensity distribution produced by electron bombardment of a single crystal Ag anode over a far-field hemisphere to parts in $10^4$. Using simple computer analysis, we have holographically reconstructed the image of the atoms without the need for detailed crystallographic modeling. We have successfully imaged the silver atoms using both 27.6 and 19.6 keV bremsstrahlung photons.

PACS numbers: 61.10.–i, 07.85.–m, 42.40.–i, 61.14.Nm

Dennis Gabor's dream was to holographically image atoms with an external source of electrons produced using an electron microscope to focus the electrons down to a very small region in front of the sample [1]. Gabor's dream has never been fully realized because the quality of the best electromagnetic lenses is only about as good as the quality of a raindrop is for imaging visible light [2]. However, his dream has been partially realized over the past ten years using electrons produced from a very small region inside the sample as the reference wave [3]. In principle, much better holographic images can be made using x rays instead of electrons [4]. Recently, two forms of internal reference wave x-ray holography have been realized [5,6]. In this Letter, we present a third: multiwavelength bremsstrahlung x-ray holography.

The basis of bremsstrahlung x-ray holography is simple: when bremsstrahlung x-ray photons are produced inside a single crystal sample, the resulting far-field intensity pattern is a Gabor hologram [7]. The holographic reference amplitude is provided by the bremsstrahlung photons which travel directly (without scattering) to the detector, and the holographic object amplitude is provided by the bremsstrahlung photons which undergo single elastic scattering (by the object atoms) on their way to the detector. Since these two final states are indistinguishable, the direct and indirect amplitudes interfere to form a holographic interference pattern. Simple Fourier analysis can be used to reconstruct the image of the atoms around the source atom from this interference pattern.

Bremsstrahlung x-ray holography is attractive for four reasons: (1) Short wavelength x rays can be produced from low-$Z$ materials, thereby allowing higher spatial resolution than their low-energy characteristic x rays would permit. (2) The bremsstrahlung production cross section is large, allowing the measurement of holograms with a tabletop apparatus. (3) X rays interact very weakly with atoms compared to electrons and thereby avoid the strong multiple-scattering problems present in the electron holographies. (4) The bremsstrahlung spectrum is continuous and, consequently, many holograms can be made simultaneously at different photon energies; these multiwavelength holograms may be combined to produce much better quality reconstructions than single energy holograms [8]. Extensive numerical simulations have demonstrated the feasibility of bremsstrahlung x-ray holography [9].

Figure 1 shows a schematic of the experimental apparatus. A tungsten filament was used to provide electrons which were accelerated toward the single crystal silver anode by a 40 kV bias. The interaction of the electrons with the target atoms produced both characteristic and bremsstrahlung photons. The target and the electron gun were housed in a vacuum enclosure maintained at $10^{-8}$ torr. The x rays exited the vacuum system through a 0.020 inch thick, semicylindrical beryllium window. The experimental apparatus has been described in detail elsewhere [10].

Although, the x-ray production efficiencies are small (about $10^{-3}$), so that most of the electron's energy is converted into heat inside the anode, a modest electron beam current of 10 mA still produces about $6 \times 10^{13}$ x-ray photons into $4\pi$ steradians. A recirculating chiller system was used to flow water at 10 °C across the back side of the sample to prevent overheating, since the electron heating would change the lattice spacing, reduce the amplitude of the holograms, and distort or melt the sample.

We used a silver single crystal to demonstrate and develop bremsstrahlung holography. Silver is an excellent

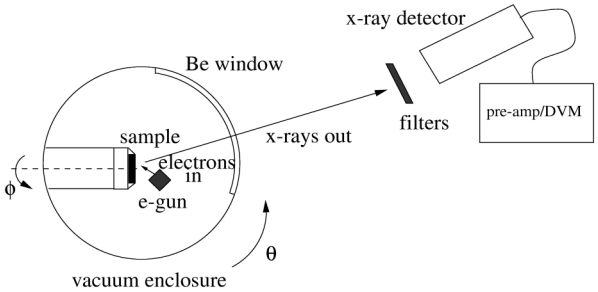


FIG. 1. Schematic of the x-ray holography experimental apparatus. The x rays produced inside the sample exit the vacuum chamber through a beryllium window. They are first energy filtered and then detected. The far-field hemisphere is measured by rotating the crystal 360° about its azimuthal axis $\phi$ and by rotating the vacuum chamber 90° about its polar axis $\theta$. The detectors remain fixed in space.

0031-9007/99/83(14)/2741(4)$15.00  

electrical and thermal conductor. In addition, silver has a reasonably high melting point (961 °C), and a relatively high atomic number ($Z = 47$). Silver has a face-centered cubic structure with a room temperature lattice constant of $a = 4.0856$ Å. The crystal we used as the anode was a disk 1.5 mm thick and 12 mm in diameter; its surface normal was oriented along the 001 crystal axis to within 0.5°.

The holographic information is contained in the variations of the measured intensities for different outgoing photon directions. As a result, we need two angular degrees of freedom to cover the surface of the far-field sphere. The most convenient way to cover this surface is to rotate the sample inside the vacuum chamber to vary the azimuthal angle $\phi$, and to rotate the entire vacuum chamber to vary the polar angle $\theta$.

The photon interference necessary for atomic resolution holography requires sufficiently monochromatic photons. The longitudinal coherence length $l_c$ of the beam is directly related to the energy distribution, $l_c = hc/\Delta E$, and this is approximately the maximum distance over which we will be able to image the neighboring atoms. This issue is particularly important for bremsstrahlung holography, where we need to eliminate the relatively intense characteristic fluorescence radiation, select a narrow energy region from the continuous bremsstrahlung spectrum, and maintain sufficient photon flux for the experiment even after the energy filtering.

To energy filter the bremsstrahlung photons we used balanced Ross filters [11]. The Ross balanced-filter technique uses a combination of two filters made of materials with a small difference in their atomic numbers. This technique relies on the fact that the x-ray absorption coefficients for elements with nearby $Z$'s vary in approximately the same way versus photon energy, except near the absorption edges. If the filter thicknesses are adjusted properly (see Fig. 2), the difference signal will provide a narrow energy bandpass signal. We measure the transmitted beam first through one filter and then through the other filter, and then we take the difference between these two signals.

Two sets of balanced-filter pairs were used: silver and tin provided a passband 3.7 keV wide centered at $E = 27.6$ keV; niobium and molybdenum provided a passband 1.0 keV wide centered at $E = 19.6$ keV. Figure 2 shows the measured signal transmitted through each filter measured with a solid state Si detector, the calculated transmission factor of the filters [12], and the measured difference signal for the Ag/Sn pair. Note that the cancellation is not perfect at low energies and that this will introduce an additional source of noise in the measured hologram. The filters were mounted on a linear translation stage which moved them in and out of the beam under computer control. The x rays were detected using NaI scintillators operated in current mode.

We measured the intensity of the x rays over an entire hemisphere, varying $\theta$ and $\phi$ in 1° steps, from $\theta = 0°$ to $\theta = 90°$, and from $\phi = 0°$ to $\phi = 360°$. With a measuring time of 2.5 sec, about $1.5 \times 10^9$ photons per point were detected. Holograms at two different energies were measured simultaneously to allow direct intercomparisons.

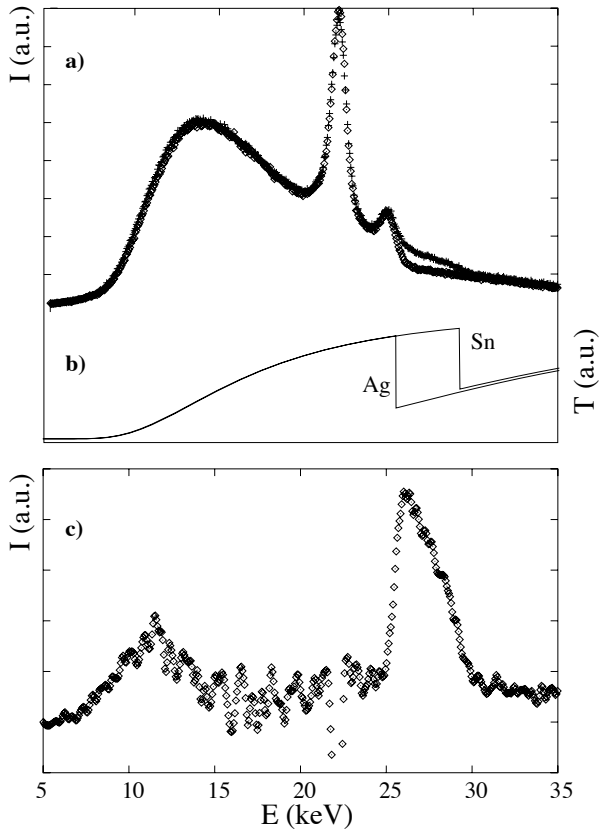


FIG. 2. Operation of the Ross filters measured with a Si detector for the Ag/Sn filter pair. (a) The measured transmission signals. Note that they match well, except in the passband. (b) The calculated energy-dependent transmission factors for the Ag and Sn filters. (c) The measured energy passband for the Ag/Sn pair.

The background was predicted to be uniform and $10^3$ times larger than the holographic fringes. To extract the hologram from the measured data — and to correct it for long term fluctuations and sample absorption — we used an area-normalization technique. First, we normalized the data so that curves of constant $\phi$ had the same integrated area. Then we normalized the (already $\phi$ normalized) curves of constant $\theta$ in the same way. This area-normalization technique very effectively filtered out fluctuations whose time scales were greater than 0.18 mHz. Slow variations in the x-ray intensity due to tungsten deposition on the target, scintillator temperature changes, and barometric pressure changes were all greatly reduced. However, this normalization technique also removed all azimuthally symmetric information from the data, thereby removing all of the interference fringes from atoms along the 001 direction.

The $\theta$ and $\phi$ area-normalized, background-subtracted signal for the data measured using the Ag/Sn filter pair

was about 0.5% of the background level. This was in good agreement with numerical simulations [9]. However, in the case of the Mo/Nb pair, the amplitude of the area-normalized background-subtracted hologram was about 2% of the background. This was larger than the simulations, and indicated additional noise. Fortunately, this extra noise was at different frequencies than the atomic signals, and consequently was separated from the atomic signals by the Fourier filter in the reconstruction algorithm.

To reconstruct the hologram we used Barton's algorithm [13]

$$\psi(\mathbf{r}) = \frac{1}{2\pi R^2} \int \chi(\mathbf{k}) e^{-i\mathbf{k}\cdot\mathbf{r}} \sin\theta \, d\theta \, d\phi$$

to obtain our holographic images of the atoms inside the silver crystal. In this equation, the measured hologram is denoted $\chi(\mathbf{k})$ where $\mathbf{k}$ is the outgoing photon wave vector. To avoid interpolating our data, we used slow Fourier transforms (simple numerical integration) directly on the grid of our data.

Figure 3 shows our reconstructions at different $z$ levels for the hologram measured using the Ag/Sn filters. The reconstruction at $z = 0$ shows four bright spots 4.0 ± 0.2 Å apart in good agreement with the expected value of 4.086 Å. Near the origin there are strong artifacts, which correspond to low spatial frequency noise due to our inability to remove all of the background. The dark spot at the center is related to the area-normalization procedure described above. Some artifacts are also present near the origin in the numerical simulations (see Fig. 5 below), yet these are much weaker and are due to small errors inherent in the single-energy reconstruction technique. The reconstruction at $z = a/2 = 2.043$ Å shows multiple bright spots, most of which do not correspond to atomic images (see below). However, the four spots closest to the center do represent atoms. Their orientation and separation (2.98 ± 0.16 Å) agree with the known structure and known orientation of the crystal in our apparatus. The reconstruction at $z = -a/2$ shows identical features, as expected because of the inversion symmetry with respect to the origin of single-energy holograms. The reconstruction at $z = a = 4.0856$ Å (not shown here) does not show any features corresponding to atoms. Contributions to the interference fringes from atoms farther than the nearest neighbors were too small to be detected due to the limited longitudinal coherence length of the bremsstrahlung photons and the falloff of the reference wave away from the source [9]. Reconstructions at intermediate $z$ levels did not show any features.

Figure 4 shows the same reconstructions for the hologram measured using the Mo/Nb filters. As expected from the narrower passband of this filter pair, these images have better resolution, and the atoms are closer to their expected positions. Other than this, they have essentially the same features as the reconstructions for the Ag/Sn hologram. The $z = 0$ level shows four atoms, 4.1 ± 0.1 Å apart. Again, there are spurious images near the center. The reconstruction at $z = a/2$ clearly shows four atoms separated by 2.87 ± 0.15 Å again in agreement with the known values. As in Fig. 3, there are extra spots that do

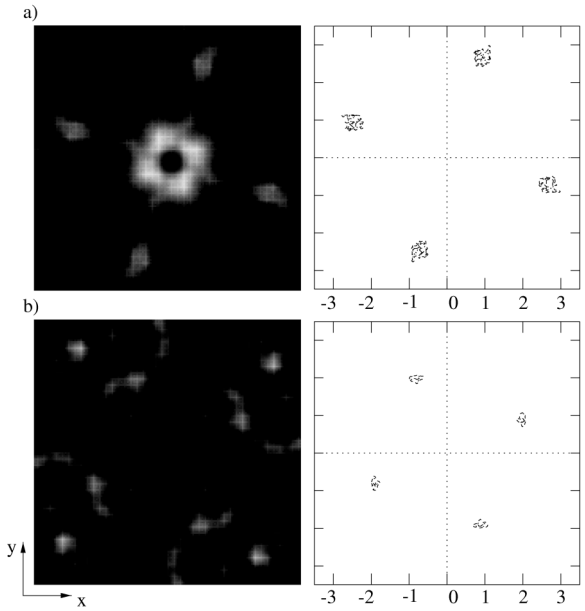


FIG. 3. Reconstructions of the hologram measured with the Ag/Sn filter pair. Each side of the square is 7 Å. (a) Results for the $z = 0$ level. There are four bright atomic images 4.0 ± 0.2 Å apart, and some spurious images near the center. (b) Results for the $z = a/2$ level. The four atoms separated by 2.98 ± 0.16 Å can clearly be distinguished.

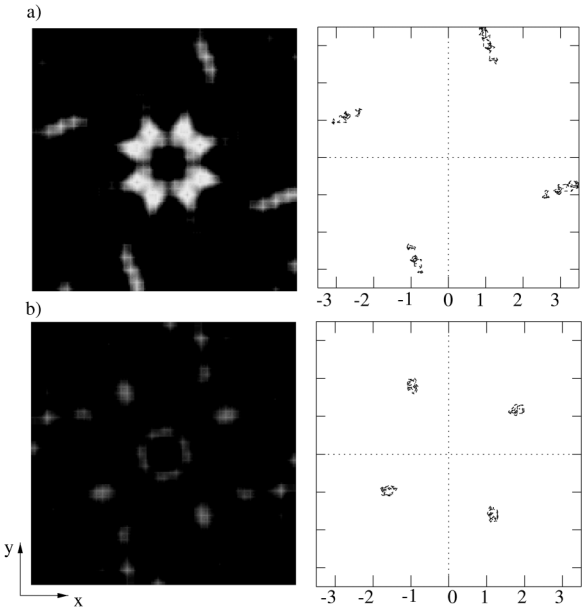


FIG. 4. Reconstructions of the hologram measured with the Mo/Nb filter pair. Each side of the square is 7 Å. (a) Results for the $z = 0$ level. There are four bright atomic images 4.1 ± 0.1 Å apart, and some spurious images near the center. (b) Results for the $z = a/2$ level. The four atoms separated by 2.87 ± 0.15 Å can clearly be distinguished.

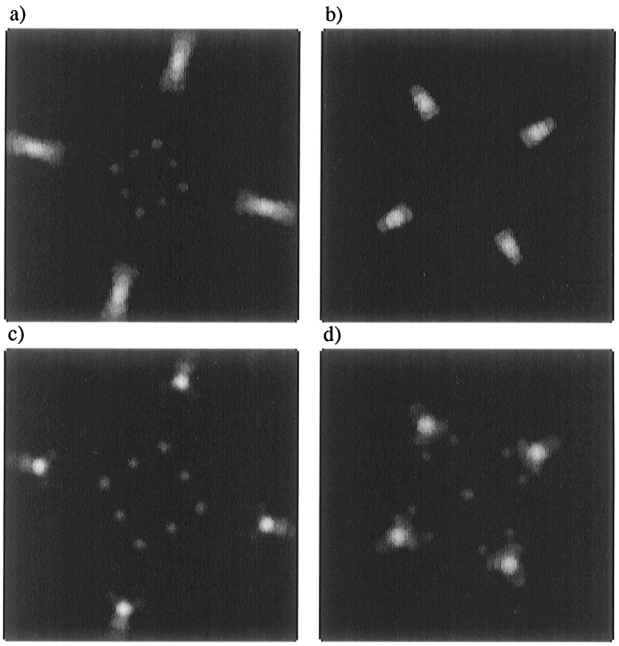


FIG. 5. Reconstructions of the numerically simulated holograms for 22 atom silver clusters [9]. Each side of the square is 7 Å. (a) Reconstruction for the Ag/Sn simulation at $z = 0$. (b) For the Ag/Sn simulation at $z = a/2$. (c) For the Mo/Nb simulation at $z = 0$. (d) For the Mo/Nb simulation at $z = a/2$.

not represent atoms. These are due to noise in the data, and can be safely discarded since they appear at different positions for different x-ray energies.

Figure 5 shows reconstructions of holograms numerically simulated for 22 atom clusters. These simulations included the anisotropic nature of the bremsstrahlung reference wave, the effects of finite energy resolution, the effects of finite angular resolution, and a holographic Debye-Waller factor [9]. Panels 5(a) and 5(b) show the reconstructions for the Ag/Sn pair, and panels 5(c) and 5(d) show the reconstructions for the Mo/Nb pair. These reconstructions agree well with the holographic reconstructions calculated from the data.

In conclusion, we have developed a new technique, bremsstrahlung x-ray holography, to image the atoms inside a crystal. From the measured far-field interference pattern, we have successfully imaged the nearest-neighbor atoms inside a silver crystal using Barton's holographic reconstruction procedure. This work demonstrates the feasibility of this technique to provide atomic structures without detailed modeling.

What is the future of these new x-ray holographies? Will they grow up to be healthy and strong x-ray structural tools? Only time will tell, but it seems clear that great improvements are possible — and will be needed — before these techniques are mature.

We thank Gerald Miller and Dennis Yee for their help during the early stages of this project. We gratefully acknowledge the partial support of this work by the Japanese New Energy and Industrial Technology Development Organization and by the Graduate Research Fund of the University of Washington.

*Current address: Department of Physics, University of Florida, Box 118440, Gainesville, Florida 32611-8440.

[1] D. Gabor, Nature (London) **161**, 777 (1948).
[2] The aberrations of electron lenses cannot be compensated because there are no magnetic monopoles; Maxwell's equations predict only positive aberrations.
[3] For a recent review of electron holography, see C.S. Fadley *et al.,* Prog. Surf. Sci. **54**, 341 (1997).
[4] C.S. Fadley, *Applications of Synchrotron Radiation Techniques to Materials Science,* MRS Symposia Proceedings No. 307 (Materials Research Society, Pittsburgh, 1993).
[5] M. Tegze and G. Faigel, Nature (London) **380**, 49 (1996).
[6] T. Gog *et al.,* Phys. Rev. Lett. **76**, 3132 (1996).
[7] G.A. Miller and L.B. Sorensen, Phys. Rev. B **56**, 2399 (1997).
[8] J.J. Barton, Phys. Rev. Lett. **67**, 3106 (1991).
[9] S.G. Bompadre, Ph.D. dissertation, University of Washington, 1998.
[10] T.W. Petersen, Ph.D. dissertation, University of Washington, 1997.
[11] P. Kirkpatrick, Phys. Rev. **10**, 186 (1939).
[12] W.H. McMaster *et al., Compilation of X-ray Cross Sections,* Lawrence Radiation Laboratory Report UCRL-50174 (National Bureau of Standards, Springfield, Virginia, 1969).
[13] J.J. Barton, Phys. Rev. Lett. **61**, 1356 (1988).